The gut contractile organoid: a novel model for studying the gut motility regulated by coordinating signals between interstitial cells of Cajal and smooth muscles

Rei Yagasaki[1,2], Ryo Nakamura[1,3], Yuuki Shikaya[1,4], Ryosuke Tadokoro[1,5], Ruolin Hao[6,7], Zhe Wang[6,7], Mototsugu Eiraku[6,7], Masafumi Inaba[1] and Yoshiko Takahashi[1,8]

1: Department of Zoology, Graduate School of Science, Kyoto University Sakyo-ku, Kyoto 606-8502, Japan
2: Present Address: WPI Nano Life Science Institute (WPI-NanoLSI), Kanazawa University, Kakuma-machi, Kanazawa 920-1192, Japan
3: Present Address: Ushimado Marine Institute, Okayama University, Setouchi, Okayama 701-4303, Japan
4: Present Address: Graduate School of Science, University of Hyogo, Kamigori-cho, Hyogo 678-1297, Japan
5: Present Address: Department of Bioscience, Okayama University of Science, Okayama, Japan
6: Institute for Life and Medical Sciences, Kyoto University, Sakyo-ku, Kyoto 606-8507, Japan
7: Department of Polymer Chemistry, Graduate School of Engineering, Kyoto University, Kyoto 615-8510, Japan
8: Author to whom all correspondence should be addressed.
email: yotayota@develop.zool.kyoto-u.ac.jp

Keywords:
gut contraction, interstitial cells of Cajal, smooth muscle cells, organoid, gap junction

Abstract

The gut undergoes peristaltic movements regulated by intricate cellular interactions. How these interactions emerge in the developing gut remains poorly explored due to a lack of model system. We here developed a novel contractile organoid that is derived from the muscle layer of chicken embryonic hindgut. The organoid contained smooth muscle cells (SMCs) and interstitial cells of Cajal (ICCs; pacemaker) with few enteric neurons, and underwent periodic contractions. The organoid was formed by self-organization with morphological arrangements of ICCs (internal) and SMCs (peripheral), allowing identification of these cells in live. GCaMP-Ca^{2+} imaging analyses revealed that Ca^{2+} transients between ICC-ICC, SMC-SMC or SMC-ICC were markedly coordinated. Pharmacological studies further suggested a role of gap junctions in ICC-to-SMC signaling, and also possible mechanical feedback from SMC's contraction to ICC's pace-making activities. In addition, two organoids with different rhythm became synchronized when mediated by SMCs, unveiling a novel contribution of SMCs to ICC's pace-making. The gut contractile organoid developed in this study offers a useful model to understand how the rhythm coordination between/among ICCs and SMCs is regulated and maintained during gut development.

Introduction

In the gut, ingested material is conveyed properly along the gut axis by the gut movements called peristalsis, which is recognized as wave-like propagation of a local constriction. The physiology of gut peristalsis has extensively been studied in adults, where the peristalsis plays pivotal roles in effective transportation and digestion/absorption of inter-luminal contents. And many cases of gut-related pathology are associated with peristaltic disfunctions. The gut peristaltic movements are achieved by intricate regulations of intercellular functions among multiple cell types. At the site of origin of peristaltic waves (OPW), a local constriction emerges along the circumferential axis, and this is soon followed by a progressive wave of the contraction along the gut axis. During these processes, the circumferential constriction demands multiple SMCs to achieve simultaneous contraction. However, due to the complex structure of the gut, how such synchronization/coordination in SMCs is regulated remains largely undetermined.

It is known in vertebrates that the embryonic gut undergoes peristaltic movements even without experience of food intake. The embryonic gut therefore serves as a powerful model to study the intrinsic mechanisms underlying the peristalsis contrasting with the adult gut where ingested content influences the gut motility increasing complexity in analyses. We have recently reported using chicken embryos that sites of OPW are randomly distributed along the gut axis at early stages, and they later become confined to specific sites, and that this confinement of OPWs enables rhythmic and patterned peristaltic movements (Shikaya et al., 2022). One of the long-standing and important questions is how the synchronized/coordinated contraction is achieved and maintained.

In a long history of gut motility studies, it has been known that enteric nervous system (ENS), smooth muscle cells (SMCs) and interstitial cells of Cajal (ICCs) play important roles in peristaltic movements (Barajas-Lopez et al., 1989; Camborova et al., 2003; Chevalier et al., 2020; Huizinga et al., 1995; Kito et al., 2005; Liu et al., 1998; Rumessen & Thuneberg, 1996; Sanders et al., 1991; Takaki, 2003; Takayama et al., 2002; Thomsen et al., 1998). It has widely been accepted that: 1) at early embryonic stages, gut movement/peristalsis does not require ENS activity, 2) ICCs serve as a pacemaker dictating their rhythm to SMCs, 3) the contraction is executed by SMC and not by ICCs, since thick fibers of myosin are found solely in SMCs. A series of elaborate electrophysiological studies showed that slow waves (a type of changes in membrane potential characteristic of gut movements) occur spontaneously in ICCs but not in SMCs, and that these slow waves lead to voltage-dependent Ca^{2+} influx evoking action potential, which is somehow transmitted to SMCs to execute gut contraction in register with ICC's

84 pace-making rhythm (Baker et al., 2021; Torihashi et al., 2002). The knowledge that ICCs
85 act as a pacemaker was supported by compelling evidence obtained by c-Kit-deficient
86 mouse mutants (W/W^v), in which ICC differentiation was severely affected leading to a
87 failure of gut peristalsis (Huizinga et al., 1995; Torihashi et al., 1999). However, it
88 remains largely unexplored how the intrinsic/spontaneous rhythm in a single ICC
89 becomes synchronized among multiple ICCs which constitute intricate networks in the
90 gut. It has also been under debate to what extend the gap junction contributes to cell-cell
91 communications between ICCs, SMCs or ICC-SMC. One reason is that it has been
92 difficult to stably maintain SMCs and ICCs in cell culture condition, and also to
93 distinguish ICCs from SMCs in the living gut (these two types of cells originate from the
94 same progenitor of splanchnopleural mesoderm during development). Thus, a novel
95 model system has been awaited to circumvent these obstacles. Recently, it was reported
96 that differentiation states of mouse hindgut-derived cells were successfully maintained
97 for a relatively long period of time in a serum-free culture medium (Wang et al., 2018).
98 In that study, many types of gut-derived cells including not only ENS, ICC, SMCs but
99 also glial cells and serosa were observed, and this large and complex cell mass was seen
100 to undergo rhythmic contractions *in vitro*.
101 It has widely been appreciated that organoids can serve as a powerful model and
102 tool to circumvent such obstacles of organ complexity. Relatively simple structures of
103 organoids allow analyses at higher resolution than *in vivo*, and also permit analyses of
104 cell behaviors in three-dimensional (3D) environment, which might be different from
105 behaviors *in vitro* confined to two dimensions. In the current study, we have developed a
106 novel organoid called "gut contractile organoid" by culturing chicken hindgut-derived
107 cells in a serum-free medium. The gut contractile organoid undergoes periodic
108 contractions, and it is essentially composed of ICCs and SMCs, the former residing
109 centrally whereas the latter peripherally, allowing distinction between the two cell types
110 in living organoids. These advantages enabled GCaMP-live imaging of Ca^{2+} dynamics,
111 and revealed coordinated oscillations of Ca^{2+} transients between ICC-ICC, SMC-SMC
112 and SMC-ICC. Pharmacological studies further suggested a role of gap junctions in an
113 ICC-to-SMC signaling, and also a possible mechanical feedback from SMC's
114 contractions to ICC's pace-making activities. In addition, by regarding an organoid as a
115 single oscillator unit and by placing these oscillators separately in a hydrogel mold, we
116 found that two oscillators with different rhythm become synchronized when mediated by
117 SMCs, supporting the notion of SMC's contribution to ICC's pace-making. The gut
118 contractile organoid developed in this study must be useful to unveil the intrinsic

mechanisms underlying the rhythm coordination and its maintenance between/among ICCs and SMCs during peristaltic movements in the embryonic gut.

Results

Spheroids were formed from muscle layer-derived cells of the embryonic hindgut

To develop a culture condition that would facilitate analyses of gut motility, we dissected the muscle layer (also called *tunica muscularis*) from the hindgut of chicken embryos of embryonic day 15 (E15) by removing the serosa and intestinal epithelium (mucosa) (Fig. S1). The isolated muscle layer was dissociated into single cells to prepare 5.0×10^5 cells per culture dish. We started analyses with a culture condition with FBS-free medium and Matrigel as substrate as previously described for cultures in mice of gastrointestinal cells including serosa (Wang et al., 2018). We tested three kinds of FBS-free media: DMEM/Ham's F-12, Ham's F-12, and Neurobasal media (see Materials and Methods). When cultured in DMEM/Ham's F-12 or Ham's F-12, dissociated cells formed very small aggregates containing several cells at day 1, the morphology of which did not change significantly until day 5 (Fig. 1A). In clear contrast, when cultured in the Neurobasal medium, cells formed clusters that were interconnected by elongated cells with neighboring clusters as early as day 1. These clusters grew as larger aggregates by day 3, and became spherical by day 5. Such spheroids were not observed in the conditions with Ham's F-12 or DMEM/Ham's F-12. We also tested different substrates, Poly-Lysine or collagen for dish coating with the Neurobasal medium, but neither one yielded spheroid. To know how the spherical aggregates were formed under the condition of Neurobasal medium and Matrigel, we obtained time-lapse images at two-hour intervals. Originally sparse clusters that were loosely connected by elongated cells merged each other forming progressively larger clusters (Fig. 1B, Movie 1). In the following experiments, we focused on the spheroids formed under the condition of Neurobasal medium and Matrigel coating.

The gut muscle layer-derived spheroids displayed periodic contractions

The spheroids underwent reiterative contractions at day 3, and these contractions were observed at least until day 7 of culture (Fig. 2A for normalized intensities of 3 representative organoids for each stage, Movie 2). Time-lapse imaging of the contractions combined with quantitative assessments by MATLAB (MathWorks, see Materials and Methods) showed that interval periods between two successive peaks were 13.3 seconds (sec), 15.4 sec and 19.6 sec for cultures at day 3, day 5 and day 7, respectively (median values) (Fig. 2B; contraction intervals).

155
156
157 **The contracting spheroid was composed of ICCs and SMCs**
158 To determine the cell types comprising the spheroids, we performed
159 immunostaining with antibodies against the chicken c-Kit protein for ICCs (Yagasaki et
160 al., 2022), and αSMA and desmin for SMCs. It is known that ICCs and SMCs are derived
161 from common progenitors which are c-Kit$^+$/αSMA$^+$, and that after differentiation ICCs
162 and SMCs are c-Kit$^+$/αSMA$^-$ and c-Kit$^-$ /αSMA$^+$, respectively (Duband et al., 1993;
163 Kluppel et al., 1998). In the clusters at day 3, c-Kit$^+$/αSMA$^-$ signals were detected in the
164 internal region, and c-Kit$^+$/αSMA$^+$ signals at the periphery (Fig. 3A, Day 3), suggesting
165 that internal cells were differentiated ICCs, whereas peripheral cells were ICC/SMC
166 progenitors. At day 5 onward, c-Kit$^+$/αSMA$^-$ cells and c-Kit$^-$/αSMA$^+$ cells were
167 segregated which were located internally and peripherally, respectively (Fig. 3A, Day 5),
168 and this spatial segregation of the cells remained unchanged until day 7 (Fig. 3A, Day 7),
169 the latest stage examined in this study. The peripherally lining cells were also positive for
170 desmin staining, supporting that these cells were SMCs (Fig. 3B). Infection with RCAS-
171 GapEGFP into a forming spheroid further visualized multipolar ICCs in the internal
172 region (Fig. 3C), a morphology known to be characteristic of ICC-MY which would
173 normally reside in the layer of myenteric plexus (Mei et al., 2009; Sanders et al., 2014).
174 ICCs of a different type were also recognized, which were elongated, thin, and lining
175 underneath the peripheral SMCs (Fig. 3A, Day 7). It is possible that these were ICC-IM,
176 known to be embedded in and tightly associated with smooth muscles in the gut (Huizinga
177 et al., 2011; Iino & Horiguchi, 2006). Unexpectedly, the spheroid contained few neural
178 cells (ENS), if any, revealed by anti-Tuj1 antibody (Fig. S2A, B). Indeed, when
179 tetrodotoxin was added to culture medium, contraction intervals of organoids were
180 comparable to those of control (before the administration) (Fig. S2C) confirming little
181 contribution by ENS. We counted cell numbers of each cell type per organoid, and found
182 that contrasting with the intact gut, the proportion of SMCs was smaller than that of ICCs
183 (Fig. S2B) possibly due to a cell type-specific loss during culture preparation.
184 Since ICCs and SMCs were spatially segregated in the sphenoid, we stained with
185 anti N-cadherin antibody (E-cadherin is positive solely in the mucosa/endoderm)
186 (Graham et al., 2017; Grosse et al., 2011). N-cadherin signals were seen in the internal
187 ICCs, and not in the peripheral SMCs (Fig. 3D). Thus, it is likely that N-cadherin plays a
188 role in the segregation.
189 In summary, the hindgut-derived spheroid displays three prominent
190 characteristics: (1) a dominant occupation by ICCs and SMCs with neglectable

contribution by ENS, (2) self-organization ability of internal ICCs encapsuled by a thin layer of SMCs, (3) recurrent and stable contractions. Based on these characteristics, we designated this spheroid as "gut contractile organoid".

Contraction-associated intracellular Ca^{2+} transients were coordinated between ICCs and SMCs in the gut contractile organoid

It has been reported that Ca^{2+} dynamics are important for pacemaker activity in ICCs and contractions of SMCs. Ca^{2+} flows into ICCs via voltage-dependent Ca^{2+} channels and propagates to SMCs, causing the gut muscle contractions (Baker et al., 2021). We therefore investigated the Ca^{2+} dynamics in our gut contractile organoids. Organoid-forming cells were infected with a RCAS-vector encoding GCaMP6s, a Ca^{2+} indicator that emits EGFP fluorescence in response to Ca^{2+} influx, and mRuby3 as a reporter (Fig. 4A). GCaMP6s-organoids were subjected to time-lapse imaging analyses by confocal microscopy. As expected, the oscillatory rhythm of Ca^{2+} transients as a whole organoid was highly concomitant with that of contractions (Fig. 4B, Movie 4).

Taking advantage of the spatial segregation between ICCs (internal) and SMCs (peripheral) (Fig. 3A, B), we compared the Ca^{2+} oscillatory rhythm among ICCs and SMCs (homotypically) and between ICC-SMC (heterotypically). We set up 3 regions of interests (ROIs) in the SMC layer with one ROI corresponding to one cell, and captured the Ca^{2+} transients. The three ROIs exhibited a synchronous pattern of Ca^{2+} oscillations (Fig. 4C, SMCs). Similarly, Ca^{2+} oscillations in three ROIs in the central region (ICCs) were synchronous (Fig. 4C, ICCs). These data highlight active communications taking place intercellularly within SMCs and ICCs, respectively. We further compared Ca^{2+} oscillations between ICC-SMC by setting up one ROI in each of ICC and SMC. Again, the Ca^{2+} rhythm was synchronized between these heterotypic cell types (Fig. 4C, ICC/SMC). With a deeper scrutinization, a peak of Ca^{2+} transient in ICC preceded that in SMC with a time lag (also called latency) of 700 msec in average (Fig. 4C, ICC/SMC; Fig. 4D, 117 peaks for 14 organoids), suggestive of a signal propagation from ICC to SMC consistent with previous reports (Baker et al., 2021).

Gap junction plays a role in ICC-to-SMC signaling

Although a series of gut motility studies have proposed an importance of gap junctions, rigid evidence has been limited due to a lack of experimental model. Our gut contractile organoid should prove useful for clarifying the roles of gap junctions in the synchronous motility, since intercellular synchronization was observed between/among identifiable cells (ICCs and SMCs) in live as shown above. We performed

227 pharmacological assessments using gap junction inhibitors including carbenoxolone
228 (CBX) and 18β-glycyrrhetinic acid (18β-GA; Chevalier, 2018; Takeda et al., 2005), two
229 of the most widely used pharmacological inhibitors for gap junction studies.
230 Following inhibitor administration into day 7 culture medium, organoids were
231 allowed to rest for 30 min to exclude possible effects by the administration, for example,
232 turbulence of the medium. Contrary to our expectation, none of 100 μM concentrations
233 of CBX or 18β-GA showed detectable effects on the recurring contractions of an organoid
234 with frequency/interval comparable to the control (Fig. S3A and B, Movie 3). These
235 undetectable effects were not due to insufficient penetrance of the drugs into the organoid,
236 since the drug administration at day 3, when organoid-forming cells were still at 2D in
237 culture, also yielded undetectable effects assessed at day 7 (Fig. S3C). The inhibiting
238 activity of the drugs used here was verified using embryonic heart cultured cells (Fig.
239 S3D).
240 Such unchanged patterns were also observed for the synchronization/
241 coordination of Ca^{2+} transients either in ICCs or SMCs in experiments conducted in a
242 way similar to Fig. 4 (Fig. 5A, B, Movie 5). Same cells in an organoid were tracked for
243 their Ca^{2+} transients before and after the inhibitor administration. With a closer look,
244 however, while overall synchronization was retained between ICCs and SMCs, the
245 preceding peak of Ca^{2+} transient in ICC was abolished (Fig. 5C, D). Collectively, while
246 the contribution by gap junction to the periodic contraction and intercellular
247 synchronization in the Day 7 organoid is relatively limited, the ICC-to-SMC signals
248 require gap junction-mediated communications, at least partly.
249
250 **Blebbistatin and Nifedipine ceased organoidal contractions and oscillatory**
251 **patterns of Ca^{2+} transients**
252 Toward searching for factors that regulate the coordination between/among ICCs
253 and SMCs, we tested blebbistatin, a specific inhibitor of myosin II, which was expected
254 to cease organoidal contractions. Experimental procedures were similar to those for gap
255 junction inhibitors. We found that blebbistatin ceased periodic contractions of organoids
256 in a concentration-dependent manner: while intervals were shorter with smaller amplitude
257 at 5 μM, contractions were ceased completely at 10 μM (Fig. 6A, B, Movie 6). The 10
258 μM-treated specimens resumed contractions following medium-wash out, showing that
259 the organoids were alive (Fig. 6B).
260 We examined Ca^{2+} transients in these contraction-inhibited organoids. Markedly,
261 periodic Ca^{2+} transients were extinguished not only in SMCs but also in ICCs, yielding
262 no/little synchronous Ca^{2+} patterns among and between ICCs and SMCs (Fig. 6C-F).

263 Although a possible direct inhibition of non-muscle myosin II in ICCs cannot be excluded,
264 these findings raised an interesting possibility that the contractility feeds back to ICCs to
265 generate/maintain their periodic rhythm.
266 This notion was further corroborated by similar experiments using Nifedipine, a
267 blocker of L-type Ca^{2+} channel known to function in gut SMCs (Chevalier et al., 2024;
268 Der et al., 2000). Organoidal contractions were completely ceased by 1 μM Nifedipine,
269 and resumed after washout, at least partly (Fig. 7A, B). In Nifedipine-treated organoids,
270 Ca^{2+} transients (GCaMP) in ICCs were erased, which resumed following washout (Fig.
271 7C).
272
273 **Inter-organoidal coordination was mediated by SMCs**
274 During analyses with our novel organoids, we noticed that they easily fuse to each
275 other, suggesting that organoids grow by progressive fusion (Fig. 8A, Movie 7). This also
276 raised the possibility that the synchronous Ca^{2+} transients among organoid-constituting
277 cells (Fig. 4C) might be a consequence of phasic coordination upon the fusion of multiple
278 organoids that had shown different oscillatory phases. To test this possibility, we
279 transferred two organoids in a petri dish, and allowed them to fuse. Before the fusion,
280 Ca^{2+} oscillatory rhythm was indeed out of phase in the two organoids (Fig. 8B, Movie 8).
281 Markedly, upon fusion by 24 hours, their rhythm became in phase/synchronous (Fig. 8B,
282 Movie 8). Intriguingly, they underwent a "pause" of oscillation during fusion (see
283 Discussion).
284 Since we noticed that cellular protrusions were often observed around the time of
285 organoidal fusion, we reasoned that these cellular processes would mediate the fusion and
286 its subsequent synchronization of Ca^{2+} transients (Fig. 8D). To test this, we developed a
287 3-well hydrogel with narrow channels connecting the wells (Fig. 9A). Organoids were
288 placed separately in each well, which prevented the fusion of organoidal bodies, but
289 allowed extension of cellular processes through the narrow channels and contact with
290 each other (Fig. 9B). After 72 hours of placement of organoids, cellular processes as well
291 as several cell bodies were present within the channel, and Ca^{2+} transients became
292 synchronized among the three organoids (Fig. 9C, Movie 9). However, with careful
293 examination, we also noticed that organoid-derived cells crawled out from the wells to
294 cover the top surface of the hydrogel, connecting the three organoids (Fig. 9D). Thus,
295 another possibility was raised that these crawled out cells would mediate the inter-
296 organoidal synchronization.
297 To test this possibility, we prepared a similar 3-well hydrogel, but in this case the
298 three wells were disconnected (no channels) so that organoid-derived cellular processes

299 were not able to connect each other (Fig. 9E). By 3 days of culture, the top surface of the
300 hydrogel was indeed covered by cells in a similar way to Fig. 9D. These cells were
301 positive for αSMA but negative for c-Kit (Fig. 9F), showing that they were SMCs that
302 were somehow detached and crawled out from the peripheral layer of their "host"
303 organoids. Importantly, coincided with the top-coverage by the SMCs, the three
304 organoids in the disconnected wells displayed synchronized Ca^{2+} transients, highlighting
305 the role of SMCs in mediating coordination between organoids (Fig. 9G, Movie 10). Gap
306 junction inhibitor yielded no/little effects on the Ca^{2+} transient coordination (Fig. 9H,
307 Movie 11).
308
309 **Discussion**
310 We have developed a novel gut contractile organoid, which displays several
311 unique characteristics: 1) it undergoes recurrent contractions, 2) differentiation states of
312 ICCs (c-Kit^{+}/αSMA^{-}) and SMCs (c-Kit^{-}/αSMA^{+}) are maintained at least until day 7 in
313 the organoid, 3) the organoid is composed essentially of two types of cells, ICCs and
314 SMCs, with few ENS cells, if any, 4) ICCs (internal) and SMCs (peripheral) can be
315 distinguished for their localization in a living organoid, allowing 5) GCaMP-visualization
316 of Ca^{2+} transients and assessments of cell interactions between and among ICCs and
317 SMCs. These characteristics circumvent, at least partly, obstacles that have hampered
318 analyses in the research of gut peristalsis, such as unstable differentiation state of ICCs
319 and SMCs in cultures, and difficulties in identifying these cells in living preparations. In
320 studies of gut movements, how ICCs generate/maintain their periodic rhythm and how
321 ICCs and SMCs interact with each other have been long-standing questions, and our
322 organoids offer powerful advantages to address these fundamental questions and to
323 understand the cellular mechanisms underlying the gut contractions/peristaltic motility at
324 least in the embryonic gut.
325 Contrasting with many cases in organoid studies that aim at a *maximum*
326 recapitulation of the intact organ, our gut contractile organoid is composed of a (probably)
327 *minimum* number of cell types that suffice the generation and/or maintenance of rhythmic
328 contractions, allowing high-resolution analyses at the cellular level. For example, adding
329 ENS components to our organoid would allow the clarification of the role of ENS in the
330 gut contraction. While the majority of internal cells in the organoid are ICCs (c-
331 Kit^{+}/αSMA^{-}), the possibility cannot be excluded that platelet-derived growth factor
332 receptor-α positive (PDFGRα^{+}/c-Kit^{-}/αSMA^{-}) cells, another type of interstitial cells
333 (fibroblast-like cell) known to mediate neural activity to SMCs in the mouse gut (Sanders

334 et al., 2024; Sanders et al., 2016), are included in our organoid. Available antibody against
335 the chicken PDFGRα protein is awaited.
336
337 **Coordinated Ca^{2+} transients in ICC/SMC populations in the gut contractile**
338 **organoid**
339 Measurement and quantification analyses with ICCs and SMCs that are
340 identifiable in the living organoid revealed exquisite coordination of Ca^{2+}
341 transients/oscillation homotypically in both ICC-ICC and SMC-SMC combinations, and
342 heterotypically between SMC-ICC (Fig. 4C). Notably, a peak of Ca^{2+} transient in ICCs
343 precedes that of SMCs with a time lag (also called latency) of 700 msec, implying a
344 signaling from ICC to SMC. These observations are consistent with previous studies
345 using ICC- and SMC-specific transgenic mice that expressed GCaMP and RCaMP,
346 respectively (Baker et al., 2021). In that study, the authors assessed Ca^{2+} transients in
347 submucosal ICCs (ICC-SM) and compared them with those in their adjacent circular
348 muscles, and showed that the rise of GCaMP signal (ICC) preceded that of RCaMP
349 (SMC) with a latency of 56 +/- 14 msec. With these observations, they concluded that
350 ICC-SM sends signals to its adjacent SMC. In our study, time-lapse imaging was mostly
351 performed with 700 msec intervals. Further studies with shorter intervals are awaited to
352 know whether the latency time would be shorter than 700 msec in average in our
353 organoids.
354
355 **Contribution of gap junction to ICC-to-SMC signaling**
356 Effects by the block of gap junction by CBX or 18β-GA were relatively limited
357 in our organoid assays: organoidal contraction rhythm and synchronous patterns of Ca^{2+}
358 transients remained unchanged between SMC-SMC and ICC-ICC. In contrast, signaling
359 from ICCs to SMCs was affected, in which the preceding peak of Ca^{2+} transient in ICCs
360 was abolished. This effect was seen by CBX but not by 18β-GA (Fig. 5C, S3E). Further
361 studies are required to clarify which connexin(s) plays a role in the generation of latency.
362 The contribution of gap junction to the ICC-to-SMC signaling was previously reported in
363 mouse gut acting from intramuscular ICCs (ICC-IM) to their adjacent circular smooth
364 muscles. However, interpretation of the role of gap junction in ICC-SMC interactions, in
365 general, has been under big debate. Some studies reported that CBX or 18β-GA failed to
366 inhibit these interactions or peristaltic motilities (Komuro et al., 1996; Rohr et al., 1998;
367 Schultz et al., 2003), or that electron microscopy did not detect structures of gap junction
368 in longitudinal muscles (Cousins et al., 2003; Daniel & Wang, 1999; Gabella & Blundell,
369 1981). Contribution of gap junctions to the gut motility appears to be highly variable in

370 different regions of gastrointestinal tract, for example, stomach versus colon (Iino et al.,
371 2007; Yang et al., 2012) . And a detection of gap junction structures or mRNA/protein of
372 connexins does not necessarily mean that the gap junction is functional. Dominant
373 negative form of gap junction might be useful. Currently, ICC- or SMC-specific gene
374 manipulations in our organoid are not available, and further studies are needed. One
375 possibility is that while gap junctions are important for the onset of rhythm coordination,
376 once the rhythm is established, other mechanisms might be employed, for example,
377 mechanical feedback from muscles to ICCs (see below). Similar notion has recently been
378 shown for coordinated Ca^{2+} signaling in cardiac muscle cells (Fukui et al., 2021).
379
380 **Possible feedback from SMC's contractility to ICC's oscillatory rhythm**
381 Blebbistatin extinguished the contraction of the organoids, which was
382 concomitant with abrogation of Ca^{2+} transients in ICCs (Fig. 6). Since it has been reported
383 that thick myosin fibers necessary for the contraction are found only in SMCs but not in
384 ICCs (Gherghiceanu & Popescu, 2005; Rumessen & Thuneberg, 1991, 1996; Sun et al.,
385 2006), it is likely that ICCs do not have contractile ability. Our observations therefore
386 raise the possibility that ICC's pace-making activity requires mechanical feedback from
387 contracting SMCs. This notion is also supported by additional finding that Nifedipine, an
388 L-type Ca^{2+} channel blocker known to be expressed in SMCs (Chevalier et al., 2024; Der
389 et al., 2000), erases both organoidal contractions and Ca^{2+} transients in ICCs (Fig. 7). The
390 possibility of the SMC-to-ICC signaling is further corroborated by other findings
391 obtained in this study showing that SMCs mediate inter-organoidal rhythm coordination
392 (Fig. 9) as more discussed below.
393 It is of note that the reciprocal interactions between pace-making cells and their
394 effectors have been reported in studies of neural circuit establishment. Spontaneous
395 activities emerging in motor neurons during peristaltic locomotion of larvae in
396 *Drosophila* are regulated by feedback from their governing muscle's contractions, so that
397 motor neurons get organized to display coordinated and stable oscillatory activities (Zeng
398 et al., 2021). Thus, it is tempting to speculate that during early gut peristalsis, ICCs that
399 have initiated their spontaneous activities receive feedback from their governing SMCs
400 to generate more stable coordination of pace-making activity among ICCs. Indeed, we
401 have previously reported that in the very early embryonic gut, origins of peristaltic wave
402 (OPWs) are randomly distributed along the gut axis, but these unstable OPWs later
403 become confined to specific sites displaying more stable and coordinated pace-making
404 patterns (Shikaya et al., 2022).
405

406 **Interactions between ICCs and SMCs in the gut contractile organoid**

407 The organoid developed in this study was derived from the muscle layer (also
408 called *tunica muscularis*) of chicken E15 hindgut devoid of mucosa and serosa, in which
409 myenteric ICCs (ICC-MY), intramuscular ICCs (ICC-IM), and submucosal ICCs (ICC-
410 SM) are localized in a way similar to those in mice, shown by staining with antibody
411 against the chicken c-Kit protein (Yagasaki et al., 2022). In the current study, c-Kit
412 antibody-staining showed two types of cells in morphology in the gut contractile
413 organoid: one is multipolar and N-cad-positive ICCs located centrally, and the other is
414 ICCs that are thin in shape, N-cad negative, and lining beneath the most external layer of
415 SMCs. Based on the knowledge obtained in studies with mammalian species that ICC-
416 MY are multipolar whereas ICC-IM are bipolar and tightly associated with adjacent
417 SMCs (Huizinga et al., 2011; Iino & Horiguchi, 2006), it is conceivable in our organoids
418 that the central cells are ICC-MY, and the peripherally lining ones are ICC-IM. In
419 addition, it has been reported in mice that signaling from ICC-IM to SMCs is gap
420 junction-dependent. Collectively, our observations that gap junction-dependent signal
421 found between ICC (central ICC) and SMC in the organoid (Fig. 5C, D) could be
422 interpreted as follows: ICC-MY (central) signals to ICC-IM (second-most peripheral),
423 which in turn acts on the external SMCs mediated partly by gap junction. Such sequences
424 of signaling (ICC-MY to ICC-IM to SMCs) have also been proposed in the intact gut in
425 mammals, although rigid evidence has not been known. At present, direct comparison of
426 Ca^{2+} transients between the ICC-IM-like cells and SMCs in our organoid was technically
427 very difficult since these two cells were both thin and tightly associated each other.
428

429 **The gut contractile organoid provides useful model and tool for studying phase**
430 **coordination of oscillatory rhythm**

431 To understand the gut peristaltic movements, which reiterate at specific sites
432 along the gut axis (Shikaya et al., 2022), deciphering the mechanisms underlying the
433 coordination/synchronization of oscillators among multiple cells is critical. Exploiting the
434 finding obtained in the current study that multiple organoids easily fuse each other in vitro,
435 we have found that two organoids with different oscillatory rhythm eventually coordinate
436 their phases upon the fusion (Fig. 8). This suggests the ability of ICCs to adjust their
437 rhythm to their neighbors. It is tempting to speculate that during "pausing time" of
438 oscillation upon organoidal fusion (Fig. 8B), they might communicate each other to adjust
439 to a unified rhythm.

440 During identification of the rhythm-adjustment mediators using the 3-well
441 hydrogel (without connecting channels), SMCs that were unexpectedly crawled out from

442 the organoids and covered the top surface of the hydrogel were able to mediate the rhythm
443 coordination among organoids (Fig. 9). Whether cellular thin protrusions connected with
444 each other observed in the channel-connected 3-well hydrogel mediate the coordination
445 remains undetermined. Nevertheless, our findings have revealed a novel role of SMCs in
446 mediating rhythm coordination, and as discussed above, these support the notion of the
447 SMC-to-ICC signaling, which is unprecedented. It is unlikely that gap junction plays a
448 major role in such signaling since gap junction inhibitors yielded no detectable effects in
449 SMC-mediated organoidal phase synchronization (Fig. 9H).
450 In summary, the gut contractile organoid developed in this study serves as a
451 powerful model to study the establishment and maintenance of oscillatory rhythm (pace-
452 making) and their coordination in the multicellular systems.
453
454
455 **Materials and Methods**
456 **Chicken embryos**
457 Fertilized chicken eggs were obtained from the Yamagishi poultry farms
458 (Wakayama, Japan) and Takeuchi Farm (Nara, Japan). Embryos were staged according
459 to embryonic days. All animal experiments were conducted with the ethical approval of
460 Kyoto University (#202110).
461
462 **Culture preparation of hindgut-derived cells**
463 A hindgut was dissected from E15 chicken embryos (Fig. S1A), and cut into
464 small pieces. After treating with 25 U dispase (Fujifilm Wako, 383-02281) /phosphate
465 buffer saline (PBS: 0.14 M NaCl, 2.7 mM KCl, 10 mM Na_2HPO_4-$12H_2O$, 1.8 mM
466 KH_2PO_4) at 38.5 °C for 40 min, serosa and intestinal epithelium were removed using
467 forceps. The muscle layer was minced into smaller pieces and treated with 0.2 mg/ml
468 collagenase (Fujifilm Wako, 038-22361) and 0.25 % trypsin/PBS at 37.0 °C for 30 min.
469 The reaction was stopped with 1 % FBS/PBS followed by centrifugation at 800 rpm for
470 3 min. The pellet was resuspended and washed in PBS followed by centrifugation. They
471 were suspended in culture medium, and 5.0×10^5 cells were plated on 14-mm diameter
472 glass-bottom dishes (Matsunami, D11130H) which had been treated with undiluted
473 Matrigel (Corning, 354248) at 38.5°C for 20 min. Poly-lysine and collagen-coated dishes
474 were purchased (Matsunami, D11131H, D11134H). D-MEM /Ham's F-12 (Wako, 048-
475 29785), Ham's F-12 (Wako, 087-08335) and Neurobasal medium (Gibco, 21103-049)
476 with 1× B-27 supplement (Gibco, 17504044) and 0.5 mM L-glutamine were tested. After
477 seeding, time-lapse images were obtained with CM20 (Evident) under 5% CO_2 and

478 38.5°C with 2-hour intervals.
479
480 **Assessment of contraction in the spheroid/cluster and organoids**
481 Time-lapse images were obtained using confocal microscopy (Nikon, A1R) under
482 5% CO_2 and 38.5°C. Region of interest (ROI) was set using the Time Measurement
483 function in Nikon NIS Elements, and changes were detected in the mode "stDev Intensity"
484 and exported as individual CSV files. Bright-field changes were normalized to values
485 between 0 and 1. For drug experiments, the values in the control group were used for
486 normalization.
487 Using MATLAB (MathWorks), the changes were plotted, and peaks with a
488 minimum prominence of 0.25 and a maximum width of 10 seconds were detected as
489 contractions of spheroid/cluster or organoid using the findpeaks function. To determine
490 the contraction frequency, we analyzed intervals between contractions and displayed as
491 box plots.
492
493 **Immunocytochemistry**
494 An organoid was fixed in acetic acid/ethanol (1:5) for 10 min at room
495 temperature (RT), and washed in PBS for 10 min at RT. The specimens were
496 permeabilized in 0.1% Tween-20 in PBS for 10 min at RT, followed by washing in PBS
497 for 10 min at RT. After blocking with 1 % blocking reagent for 1 hour at RT, specimens
498 were incubated overnight at 4 ℃ with dilution of 1:300 anti-c-Kit (Yagasaki et al., 2022),
499 1:300 Tuj-1 (RSD, MAB1195), 1:400 anti-αSMA antibody (Sigma-Aldrich, A5228),
500 anti-Desmin antibody (Novus Biologicals, NBP1-97707) and/or 1:200 anti-N-cadherin
501 antibodies (TAKARA, M110) in 1% blocking regent (Roche, 1096176)/PBS. Following
502 three times washing in PBS for 10 min each at RT, specimens were incubated for 1.5 hr
503 at RT with 1:500 anti-rabbit IgG(H+L)-Alexa 488-conjugated antibody (Donkey;
504 Invitrogen, A21206), anti-mouse IgG_{2a}-Alexa 568-conjugated antibody (Goat; Invitrogen,
505 A21134), anti-rat IgG (H+L)-Alexa 488-conjugated antibody (Goat; Invitrogen, A11006)
506 and 1:2000 DAPI. After washing three times in PBS for 10 min at RT, fluorescent images
507 were obtained using the Nikon A1R confocal microscope.
508
509 **Plasmids**
510 pAAV-hSynapsin1-GCaMP6s-P2A-mRuby3 was purchased from Addgene
511 (112007). Full-length cDNA of GCaMP6s was PCR-amplified:
512 forward 5'- GCGTACCACTGTGGCATCGATGCCACCATGGGTTCTCA -3',
513 reverse 5'- GCCCGTACATCGCATCGATTTACTTGTACAGCTCGT -3'.

514 The retroviral vector RCAS-EGFP was digested with Cla I to remove EGFP, into which
515 a DNA fragment was inserted by In-Fusion HD Cloning Kit (TAKARA) to produce
516 RCAS-GCaMP6s-P2A-mRuby3. RCAS-GapEGFP is as previously described (Murai et
517 al., 2015)
518
519 **Preparation of retroviral vector particles**
520 RCAS-GCaMP6s-P2A-mRuby3 was transfected into the chicken fibroblast line
521 cells DF1 using Lipofectamin 2000 (Invitrogen). Transfected cells were cultured in 10
522 cm culture dish until confluent. The supernatant of transfected DF1 was collected for viral
523 precipitation, from which retroviral particles were prepared using Retro-Concentin™
524 Virus Precipitation Solution (SBI, RV100A-1).
525
526 **Intracellular Ca^{2+} imaging in the gut contractile organoid**
527 On day 2 or 3 of cell culture, a 10 mg/ml polybrene solution (final concentration:
528 4 μg/ml; Nacalai, 12996-81) and 20 μl of Opti-MEM containing the aforementioned viral
529 particles were added to the culture medium to transfect GCaMP6s into organoid-forming
530 cells. The culture medium was replaced with fresh medium on day 5, and Ca^{2+} imaging
531 was performed on day 7. Time-lapse images were acquired using a confocal microscope
532 (Nikon, A1R) at intervals of either 700 or 450 msec. Fluorescence intensity from each
533 region of interest (ROI) was exported into an Excel file using the time-measurement
534 function of the NIS-Elements software (Nikon). Fluorescence intensity traces were
535 plotted using the Excel data, with the start of measurement set as time zero. For peak
536 latency analysis, calcium transients in ICCs and SMCs were identified using the
537 "findpeaks" function in MATLAB (MathWorks). Temporal differences between peak
538 signals in ICC and SMC were calculated to show the latency.
539
540 **Drug administration**
541 Carbenoxolone (CBX; nacalai tesque, 32775-51) /H_2O, 18beta-Glycyrrhetinic
542 acid (18β-GA; abcam, ab142579)/DMSO, (-)-Blebbistatin (FUJIFILM Wako, 021-
543 17041) and Nifedipine (FUJIFILM Wako, 141-05783) were prepared. Time-lapse images
544 were acquired for a single organoid before and after the drug administration. Following
545 the drug adding, organoids were allowed to rest for 30 min to avoid possible effect of
546 turbulence of the medium, and time-lapse images were taken for 5 min.
547
548 **Three-well hydrogel fabrication**
549 The photoinitiator P2CK was synthesized as previously reported (Li et al., 2013).

The target product was verified using proton NMR and Bruker's TopSpin software. Gelatin-Norbornene was synthesized based on previous report (Van Hoorick et al., 2018). The final reaction mixture was transferred to a dialysis tube (5-6 kDa; Spectra Por, cat. no. 132680T) for dialysis against pure water at 40°C for 3 days. After dialysis, the solution's pH was carefully adjusted to 8.0.

A piece of 3-well hydrogel was fabricated on a glass bottom dish (Matsunami) from 100 μL of a solution containing 20 wt % Gelatin-Norbornene, 2 mM of the photoinitiator P2CK, and 20 mM of crosslinker (DTT) (TCI, #D1071) using a two-photon microscope with controllable laser power in 3D space according to the voxel file input (Olympus, in house customized). The voxel files specifying the 3D shape of the hydrogel were designed with Fusion 360 software. (Autodisk). Organoids were transferred to the hydrogel using a glass capillary.

Culture of embryonic heart-derived cells

A heart was dissected from E10 chicken embryo, and cut into small pieces. The tissue fragments were treated with 0.125% trypsin in PBS at 37.0 °C for 30 min. The reaction was terminated by adding 10 % FBS in D-MEM/Ham's F-12, followed by centrifugation at 800 rpm for 3 min. Pellet was resuspended in D-MEM/Ham's F-12 supplemented with 10% FBS, and the cells were plated in poly-L-lysine-coated glass-bottom dishes (Matsunami).

On day 1, time-lapse images were acquired using confocal microscopy under 5% CO_2 at 38.5 °C, with 700 msec intervals. Cell contractions were detected using the "stDev Intensity" mode in the Time Measurement function of Nikon NIS-Elements.

Acknowledgement

We thank Dr. Scott Gilbert for careful reading of the manuscript and discussion. We also thank National BioResource Project (Chicken-Quail, Nagoya University) for their technical help. This work was supported by JSPS KAKENHI Grant Numbers; 23H04933, 20H03259, 20K20520, 20K21425 for Y. T., and 21K06198, 23H04702 for M. I., and FY 2022 Kusunoki 125 of Kyoto University 125th Anniversary Fund for M. I., and Ginpu Funds (Kyoto University) and incu-be fund (Leave a Nest Co., Ltd.) for R. Y.. R. Y. is an ex-fellow of JSPS.

References

586 Baker, S. A., Leigh, W. A., Del Valle, G., De Yturriaga, I. F., Ward, S. M., Cobine, C. A., Drumm,
587 B. T., & Sanders, K. M. (2021). Ca(2+) signaling driving pacemaker activity in
588 submucosal interstitial cells of Cajal in the murine colon. *Elife*, *10*.
589 https://doi.org/10.7554/eLife.64099
590 Barajas-Lopez, C., Berezin, I., Daniel, E. E., & Huizinga, J. D. (1989). Pacemaker activity recorded
591 in interstitial cells of Cajal of the gastrointestinal tract. *Am J Physiol*, *257*(4 Pt 1), C830-
592 835. https://doi.org/10.1152/ajpcell.1989.257.4.C830
593 Camborova, P., Hubka, P., Sulkova, I., & Hulin, I. (2003). The pacemaker activity of interstitial
594 cells of Cajal and gastric electrical activity. *Physiol Res*, *52*(3), 275-284.
595 https://www.ncbi.nlm.nih.gov/pubmed/12790758
596 Chevalier, N. R. (2018). The first digestive movements in the embryo are mediated by
597 mechanosensitive smooth muscle calcium waves. *Philos Trans R Soc Lond B Biol Sci*,
598 *373*(1759). https://doi.org/10.1098/rstb.2017.0322
599 Chevalier, N. R., Ammouche, Y., Gomis, A., Teyssaire, C., de Santa Barbara, P., & Faure, S. (2020).
600 Shifting into high gear: how interstitial cells of Cajal change the motility pattern of the
601 developing intestine. *Am J Physiol Gastrointest Liver Physiol*, *319*(4), G519-g528.
602 https://doi.org/10.1152/ajpgi.00112.2020
603 Chevalier, N. R., Dacher, N., Jacques, C., Langlois, L., Guedj, C., & Faklaris, O. (2019).
604 Embryogenesis of the peristaltic reflex. *J Physiol*, *597*(10), 2785-2801.
605 https://doi.org/10.1113/jp277746
606 Cousins, H. M., Edwards, F. R., Hickey, H., Hill, C. E., & Hirst, G. D. (2003). Electrical coupling
607 between the myenteric interstitial cells of Cajal and adjacent muscle layers in the guinea-
608 pig gastric antrum. *J Physiol*, *550*(Pt 3), 829-844.
609 https://doi.org/10.1113/jphysiol.2003.042176
610 Daniel, E. E., & Wang, Y. F. (1999). Gap junctions in intestinal smooth muscle and interstitial
611 cells of Cajal. *Microsc Res Tech*, *47*(5), 309-320. https://doi.org/10.1002/(SICI)1097-
612 0029(19991201)47:5<309::AID-JEMT2>3.0.CO;2-K
613 Duband, J. L., Gimona, M., Scatena, M., Sartore, S., & Small, J. V. (1993). Calponin and SM 22
614 as differentiation markers of smooth muscle: spatiotemporal distribution during avian
615 embryonic development. *Differentiation*, *55*(1), 1-11. https://doi.org/10.1111/j.1432-
616 0436.1993.tb00027.x
617 Fukui, H., Chow, R. W., Xie, J., Foo, Y. Y., Yap, C. H., Minc, N., Mochizuki, N., & Vermot, J.
618 (2021). Bioelectric signaling and the control of cardiac cell identity in response to
619 mechanical forces. *Science*, *374*(6565), 351-354.
620 https://doi.org/10.1126/science.abc6229
621 Gabella, G., & Blundell, D. (1981). Gap junctions of the muscles of the small and large intestine.

622 *Cell Tissue Res*, *219*(3), 469-488. https://doi.org/10.1007/BF00209987
623 Gherghiceanu, M., & Popescu, L. M. (2005). Interstitial Cajal-like cells (ICLC) in human resting
624 mammary gland stroma. Transmission electron microscope (TEM) identification. *J Cell*
625 *Mol Med*, *9*(4), 893-910. https://doi.org/10.1111/j.1582-4934.2005.tb00387.x
626 Graham, H. K., Maina, I., Goldstein, A. M., & Nagy, N. (2017). Intestinal smooth muscle is
627 required for patterning the enteric nervous system. *J Anat*, *230*(4), 567-574.
628 https://doi.org/10.1111/joa.12583
629 Grosse, A. S., Pressprich, M. F., Curley, L. B., Hamilton, K. L., Margolis, B., Hildebrand, J. D., &
630 Gumucio, D. L. (2011). Cell dynamics in fetal intestinal epithelium: implications for
631 intestinal growth and morphogenesis. *Development*, *138*(20), 4423-4432.
632 https://doi.org/10.1242/dev.065789
633 Huizinga, J. D., Martz, S., Gil, V., Wang, X. Y., Jimenez, M., & Parsons, S. (2011). Two
634 independent networks of interstitial cells of cajal work cooperatively with the enteric
635 nervous system to create colonic motor patterns. *Front Neurosci*, *5*, 93.
636 https://doi.org/10.3389/fnins.2011.00093
637 Huizinga, J. D., Thuneberg, L., Kluppel, M., Malysz, J., Mikkelsen, H. B., & Bernstein, A. (1995).
638 W/kit gene required for interstitial cells of Cajal and for intestinal pacemaker activity.
639 *Nature*, *373*(6512), 347-349. https://doi.org/10.1038/373347a0
640 Iino, S., & Horiguchi, K. (2006). Interstitial cells of cajal are involved in neurotransmission in the
641 gastrointestinal tract. *Acta Histochem Cytochem*, *39*(6), 145-153.
642 https://doi.org/10.1267/ahc.06023
643 Iino, S., Horiguchi, S., Horiguchi, K., & Nojyo, Y. (2007). Interstitial cells of Cajal in the
644 gastrointestinal musculature of W mutant mice. *Arch Histol Cytol*, *70*(3), 163-173.
645 https://doi.org/10.1679/aohc.70.163
646 Kito, Y., Ward, S. M., & Sanders, K. M. (2005). Pacemaker potentials generated by interstitial cells
647 of Cajal in the murine intestine. *Am J Physiol Cell Physiol*, *288*(3), C710-720.
648 https://doi.org/10.1152/ajpcell.00361.2004
649 Kluppel, M., Huizinga, J. D., Malysz, J., & Bernstein, A. (1998). Developmental origin and Kit-
650 dependent development of the interstitial cells of cajal in the mammalian small intestine.
651 *Dev Dyn*, *211*(1), 60-71. https://doi.org/10.1002/(SICI)1097-
652 0177(199801)211:1<60::AID-AJA6>3.0.CO;2-5
653 Komuro, T., Tokui, K., & Zhou, D. S. (1996). Identification of the interstitial cells of Cajal. *Histol*
654 *Histopathol*, *11*(3), 769-786. https://www.ncbi.nlm.nih.gov/pubmed/8839765
655 Li, Z. Q., Torgersen, J., Ajami, A., Mühleder, S., Qin, X. H., Husinsky, W., Holnthoner, W.,
656 Ovsianikov, A., Stampfl, J., & Liska, R. (2013). Initiation efficiency and cytotoxicity of
657 novel water-soluble two-photon photoinitiators for direct 3D microfabrication of

658 hydrogels. *Rsc Advances*, *3*(36), 15939-15946. https://doi.org/10.1039/c3ra42918k
659 Liu, L. W., Thuneberg, L., & Huizinga, J. D. (1998). Development of pacemaker activity and
660 interstitial cells of Cajal in the neonatal mouse small intestine. *Dev Dyn*, *213*(3), 271-282.
661 https://doi.org/10.1002/(SICI)1097-0177(199811)213:3<271::AID-AJA4>3.0.CO;2-R
662 Mei, F., Han, J., Huang, Y., Jiang, Z. Y., Xiong, C. J., & Zhou, D. S. (2009). Plasticity of interstitial
663 cells of cajal: a study in the small intestine of adult Guinea pigs. *Anat Rec (Hoboken)*,
664 *292*(7), 985-993. https://doi.org/10.1002/ar.20928
665 Murai, H., Tadokoro, R., Sakai, K., & Takahashi, Y. (2015). In ovo gene manipulation of
666 melanocytes and their adjacent keratinocytes during skin pigmentation of chicken
667 embryos. *Dev Growth Differ*, *57*(3), 232-241. https://doi.org/10.1111/dgd.12201
668 Rohr, S., Kucera, J. P., & Kleber, A. G. (1998). Slow conduction in cardiac tissue, I: effects of a
669 reduction of excitability versus a reduction of electrical coupling on microconduction. *Circ*
670 *Res*, *83*(8), 781-794. https://doi.org/10.1161/01.res.83.8.781
671 Rumessen, J. J., & Thuneberg, L. (1991). Interstitial cells of Cajal in human small intestine.
672 Ultrastructural identification and organization between the main smooth muscle layers.
673 *Gastroenterology*, *100*(5 Pt 1), 1417-1431.
674 https://www.ncbi.nlm.nih.gov/pubmed/2013387
675 Rumessen, J. J., & Thuneberg, L. (1996). Pacemaker cells in the gastrointestinal tract: interstitial
676 cells of Cajal. *Scand J Gastroenterol Suppl*, *216*, 82-94.
677 https://doi.org/10.3109/00365529609094564
678 Sanders, K. M., Drumm, B. T., Cobine, C. A., & Baker, S. A. (2024). Ca(2+) dynamics in
679 interstitial cells: foundational mechanisms for the motor patterns in the gastrointestinal
680 tract. *Physiol Rev*, *104*(1), 329-398. https://doi.org/10.1152/physrev.00036.2022
681 Sanders, K. M., Kito, Y., Hwang, S. J., & Ward, S. M. (2016). Regulation of Gastrointestinal
682 Smooth Muscle Function by Interstitial Cells. *Physiology (Bethesda)*, *31*(5), 316-326.
683 https://doi.org/10.1152/physiol.00006.2016
684 Sanders, K. M., Publicover, N. G., & Ward, S. M. (1991). Involvement of interstitial cells of Cajal
685 in pacemaker activity of canine colon. *J Smooth Muscle Res*, *27*(1), 1-11.
686 https://doi.org/10.1540/jsmr.27.1
687 Sanders, K. M., Ward, S. M., & Koh, S. D. (2014). Interstitial cells: regulators of smooth muscle
688 function. *Physiol Rev*, *94*(3), 859-907. https://doi.org/10.1152/physrev.00037.2013
689 Schultz, T., Daniel, V., & Daniel, E. E. (2003). Does ICC pacing require functional gap junctions
690 between ICC and smooth muscle in mouse intestine? *Neurogastroenterol Motil*, *15*(2),
691 129-138. https://doi.org/10.1046/j.1365-2982.2003.00401.x
692 Shikaya, Y., Takase, Y., Tadokoro, R., Nakamura, R., Inaba, M., & Takahashi, Y. (2022).
693 Distribution Map of Peristaltic Waves in the Chicken Embryonic Gut Reveals Importance

694 of Enteric Nervous System and Inter-Region Cross Talks Along the Gut Axis. *Front Cell*
695 *Dev Biol*, *10*, 827079. https://doi.org/10.3389/fcell.2022.827079
696 Sun, X., Yu, B., Xu, L., Dong, W., & Luo, H. (2006). Interstitial cells of Cajal in the murine
697 gallbladder. *Scand J Gastroenterol*, *41*(10), 1218-1226.
698 https://doi.org/10.1080/00365520600708800
699 Takaki, M. (2003). Gut pacemaker cells: the interstitial cells of Cajal (ICC). *J Smooth Muscle Res*,
700 *39*(5), 137-161. https://doi.org/10.1540/jsmr.39.137
701 Takayama, I., Horiguchi, K., Daigo, Y., Mine, T., Fujino, M. A., & Ohno, S. (2002). The interstitial
702 cells of Cajal and a gastroenteric pacemaker system. *Arch Histol Cytol*, *65*(1), 1-26.
703 https://doi.org/10.1679/aohc.65.1
704 Takeda, Y., Ward, S. M., Sanders, K. M., & Koh, S. D. (2005). Effects of the gap junction blocker
705 glycyrrhetinic acid on gastrointestinal smooth muscle cells. *Am J Physiol Gastrointest*
706 *Liver Physiol*, *288*(4), G832-841. https://doi.org/10.1152/ajpgi.00389.2004
707 Thomsen, L., Robinson, T. L., Lee, J. C., Farraway, L. A., Hughes, M. J., Andrews, D. W., &
708 Huizinga, J. D. (1998). Interstitial cells of Cajal generate a rhythmic pacemaker current.
709 *Nat Med*, *4*(7), 848-851. https://doi.org/10.1038/nm0798-848
710 Torihashi, S., Fujimoto, T., Trost, C., & Nakayama, S. (2002). Calcium oscillation linked to
711 pacemaking of interstitial cells of Cajal: requirement of calcium influx and localization of
712 TRP4 in caveolae. *J Biol Chem*, *277*(21), 19191-19197.
713 https://doi.org/10.1074/jbc.M201728200
714 Torihashi, S., Nishi, K., Tokutomi, Y., Nishi, T., Ward, S., & Sanders, K. M. (1999). Blockade of
715 kit signaling induces transdifferentiation of interstitial cells of cajal to a smooth muscle
716 phenotype. *Gastroenterology*, *117*(1), 140-148. https://doi.org/10.1016/s0016-
717 5085(99)70560-3
718 Van Hoorick, J., Gruber, P., Markovic, M., Rollot, M., Graulus, G. J., Vagenende, M., Tromayer,
719 M., Van Erps, J., Thienpont, H., Martins, J. C., Baudis, S., Ovsianikov, A., Dubruel, P., &
720 Van Vlierberghe, S. (2018). Highly Reactive Thiol-Norbornene Photo-Click Hydrogels:
721 Toward Improved Processability. *Macromol Rapid Commun*, *39*(14), e1800181.
722 https://doi.org/10.1002/marc.201800181
723 Wang, Q., Wang, K., Solorzano-Vargas, R. S., Lin, P. Y., Walthers, C. M., Thomas, A. L., Martín,
724 M. G., & Dunn, J. C. Y. (2018). Bioengineered intestinal muscularis complexes with long-
725 term spontaneous and periodic contractions. *PLoS One*, *13*(5), e0195315.
726 https://doi.org/10.1371/journal.pone.0195315
727 Yagasaki, R., Shikaya, Y., Kawachi, T., Inaba, M., Takase, Y., & Takahashi, Y. (2022). Newly raised
728 anti-c-Kit antibody visualizes morphology of interstitial cells of Cajal in the developing
729 gut of chicken embryos. *Dev Growth Differ*, *64*(8), 446-454.

https://doi.org/10.1111/dgd.12808

Yang, P., Yu, Z., Gandahi, J. A., Bian, X., Wu, L., Liu, Y., Zhang, L., Zhang, Q., & Chen, Q. (2012). The identification of c-Kit-positive cells in the intestine of chicken. *Poult Sci*, *91*(9), 2264-2269. https://doi.org/10.3382/ps.2011-02076

Zeng, X., Komanome, Y., Kawasaki, T., Inada, K., Jonaitis, J., Pulver, S. R., Kazama, H., & Nose, A. (2021). An electrically coupled pioneer circuit enables motor development via proprioceptive feedback in Drosophila embryos. *Curr Biol*, *31*(23), 5327-5340 e5325. https://doi.org/10.1016/j.cub.2021.10.005

740 **Figure legends**

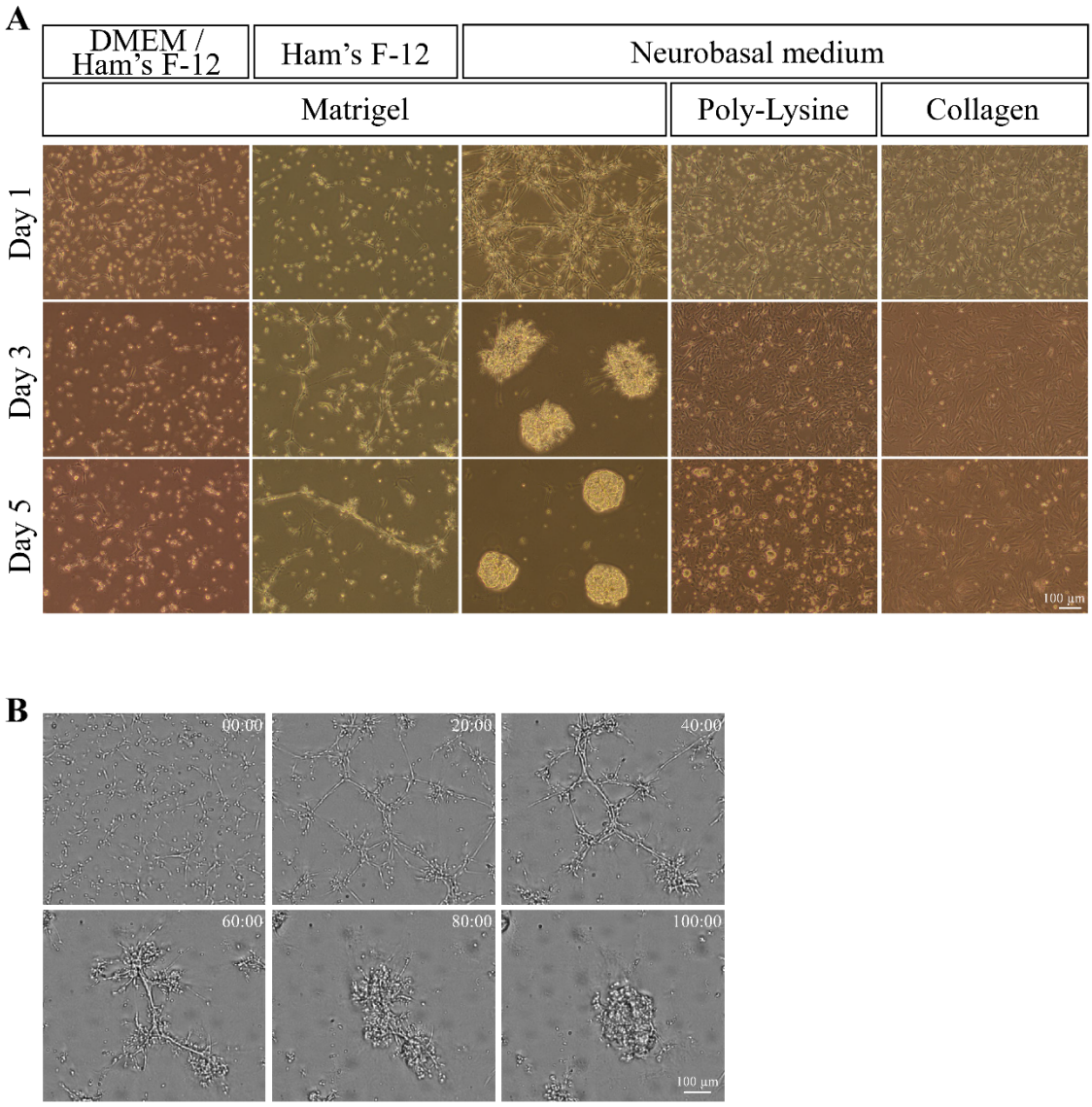

741

742 **Figure 1. Culture of muscle layer-derived cells prepared from embryonic hindgut.**
743 **(A)** Culture of muscle layer-derived cells prepared from embryonic hindgut with FBS
744 free-media and substrates. **(B)** Long-term time-lapse imaging after seeding on Matrigel
745 with Neurobasal media. The images show the ability of these cells to self-assemble at 0,
746 20, 40, 60, 80 and 100 hours taken from Movie 1. Scale bars: 100 µm (A, B).
747

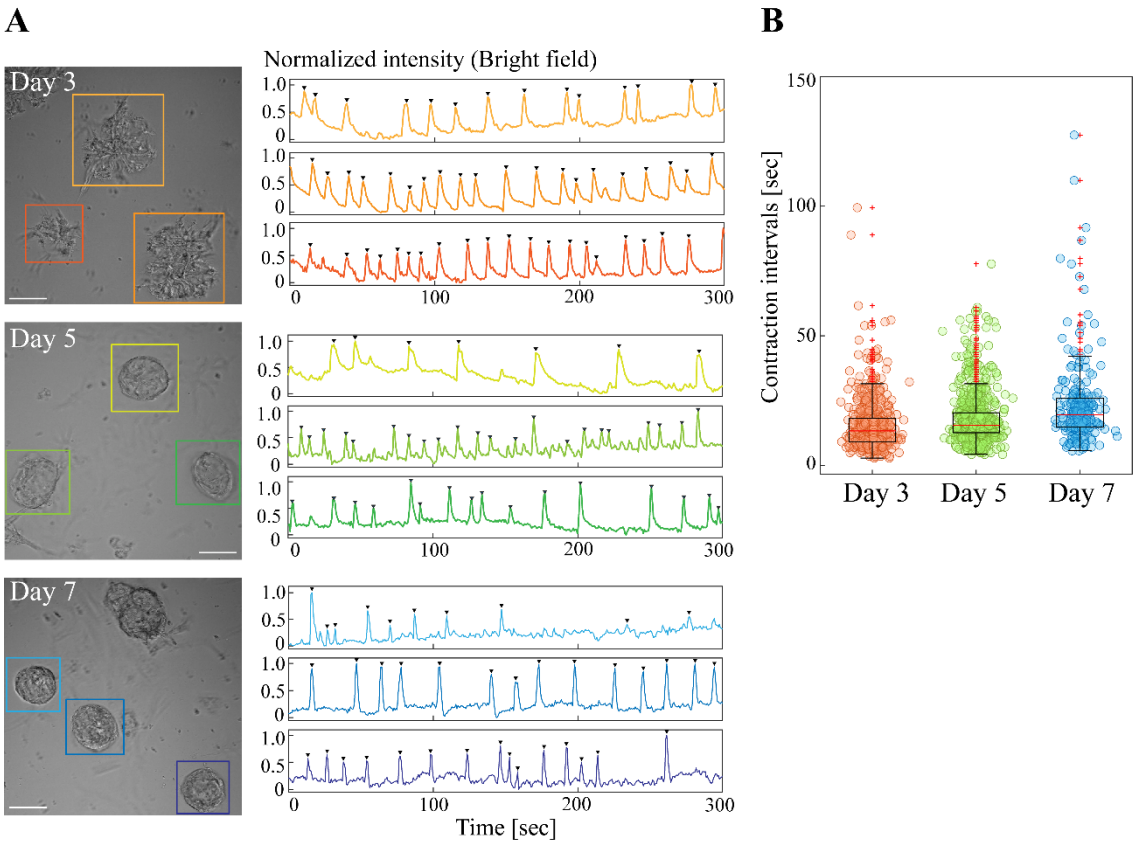

Figure 2. Spheroids formed in Neurobasal medium and Matrigel exhibited reiterated contractions.

(A) Clusters/spheroids at days 3, 5, and 7 exhibited reiterative contractions. Graphs show normalized contraction intensities visualized using the Time Measurement function. Arrowheads indicate contraction peaks defined by a peak prominence > 0.25 and a peak width ≤ 10 seconds. **(B)** Contraction intervals in clusters/spheroids from day 3 to day 7. Each dot represents a single contraction interval. Median values: day 3, 13.3; day 5, 15.4; day 7, 19.6. Sample sizes: day 3, $n = 35$, peak count = 646; day 5, $n = 48$, peak count = 748; day 7, $n = 21$, peak count = 250. Scale bar: 50 μm (A).

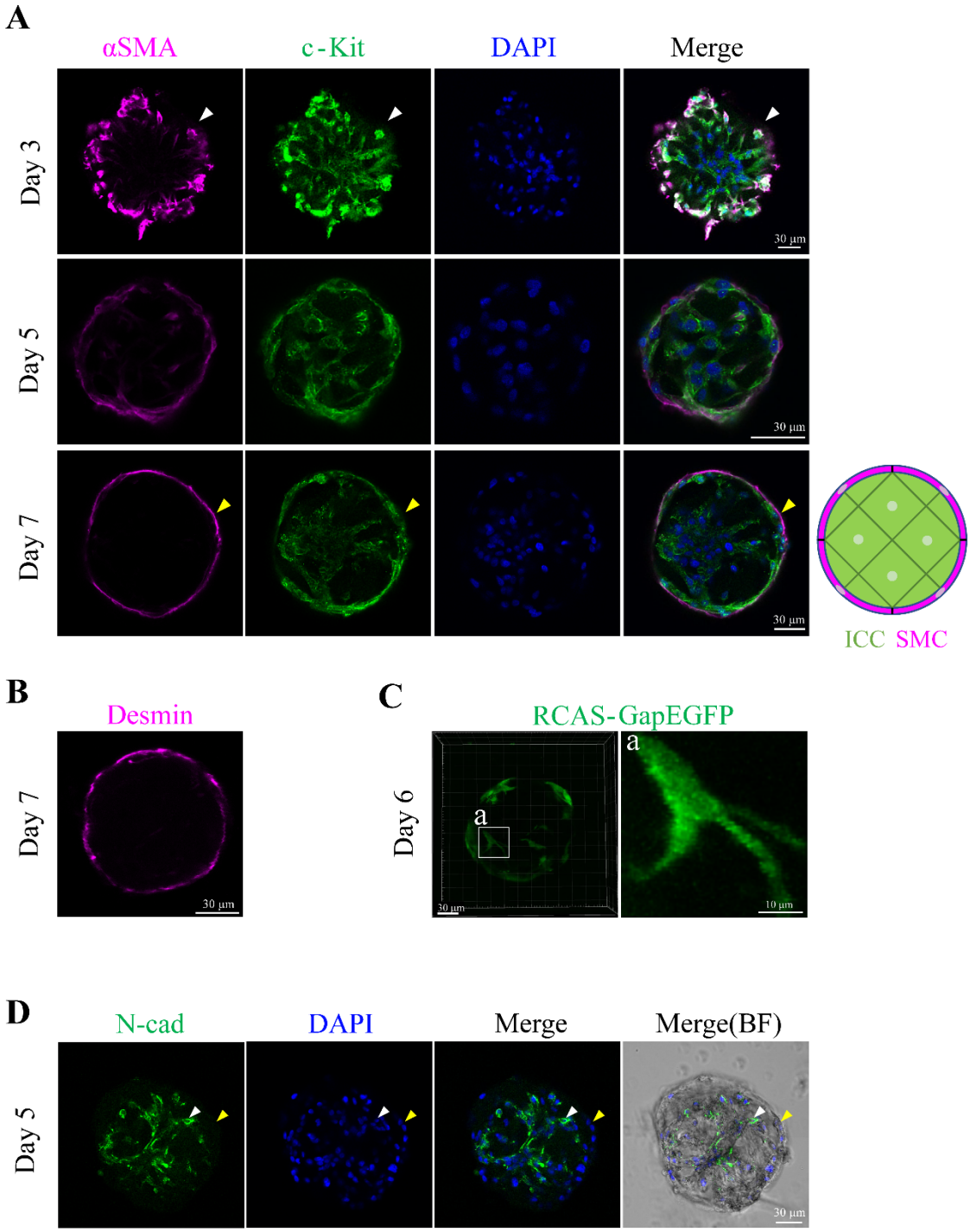

759

760 **Figure 3. Clusters/spheroids are composed of internally located ICCs and**
761 **peripherally located SMCs.**

762 **(A)** Co-staining with anti-c-Kit and anti-αSMA antibodies. White arrowheads indicate
763 co-expression of c-Kit and αSMA at day 3. Yellow arrowheads indicate cells expressing
764 αSMA but not c-Kit at day 7. A schematic diagram illustrates the spatial arrangement of

765 cells within a day 7 spheroid (green: ICCs; magenta: SMCs). **(B)** Staining with anti-
766 Desmin antibody, a marker for mature smooth muscle cells. **(C)** Cell morphology within
767 the spheroid at day 6 visualized by RCAS-gapEGFP expression. **(D)** Staining of day 5
768 spheroids with anti-N-cadherin antibody. A white arrowhead indicates N-cadherin–
769 positive cells, while a yellow arrowhead indicates N-cadherin–negative cells in the outer
770 region of the spheroid. Scale bars: 30 µm (A–D), 10 µm (inset a in C).

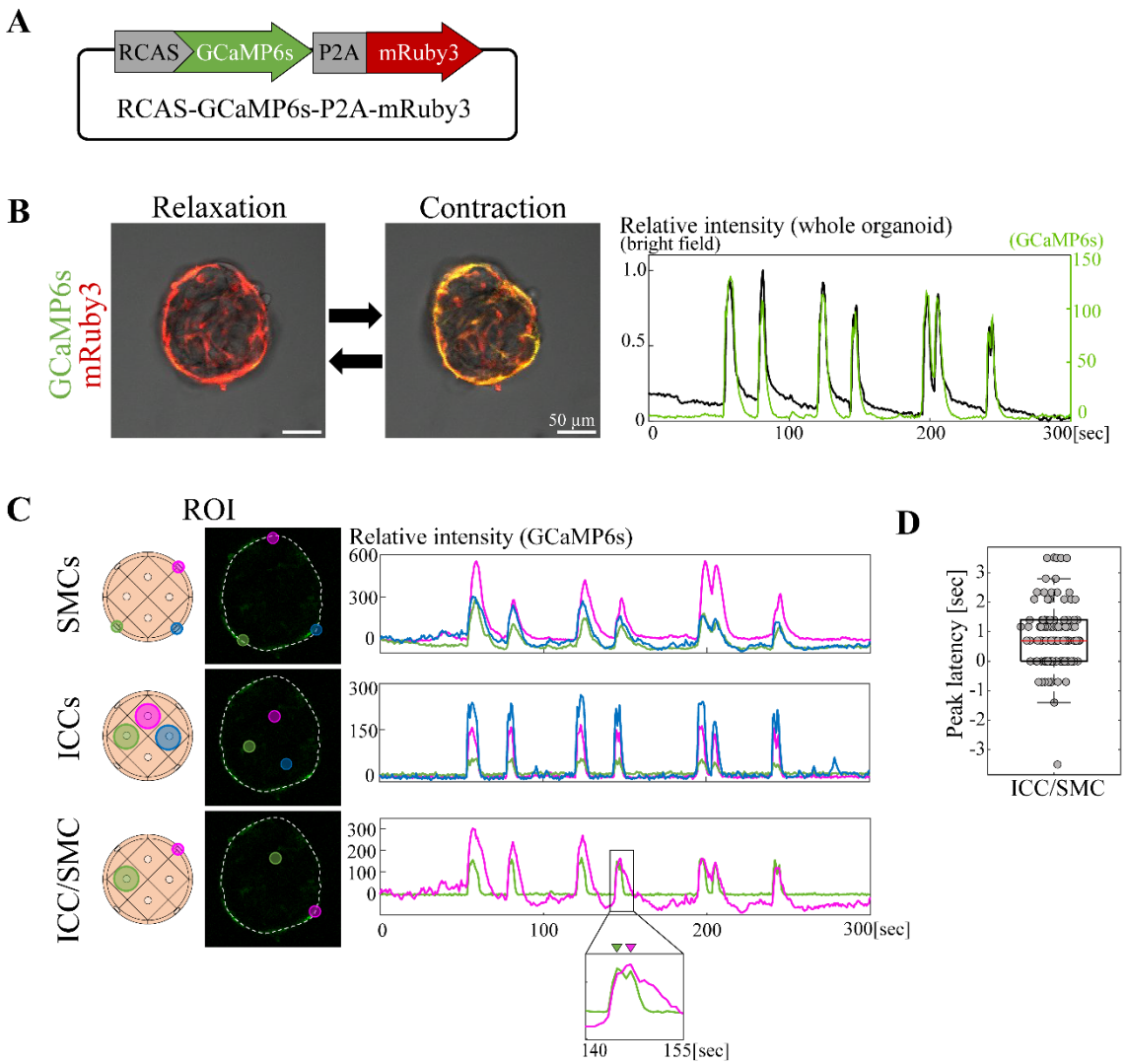

Figure 4. Ca^{2+} imaging of the gut contractile organoid revealed intercellular synchronization.

(A) RCAS-GCaMP6s-P2A-mRuby3 plasmid. **(B)** Ca^{2+} imaging of gut contractile organoid during relaxation and contraction. Ca^{2+} dynamics (green) and normalized values of contraction (grey) of gut contractile organoid. **(C)** Simultaneous measurement of intercellular Ca^{2+} dynamics between ICC-ICC, SMC-SMC or ICC-SMC. Three or two ROIs in Ca^{2+} signal-positive cells were set in a single organoid. Graphs show Ca^{2+} dynamics in the ROIs. Magnified view shows that a peak of Ca^{2+} signal in ICC (green) preceded that in SMC (magenta). **(D)** Peak latency in ICC/SMC. Median value = 0.7; Sample size: $n = 14$, peak count = 117. Scale bar: 50 µm (B).

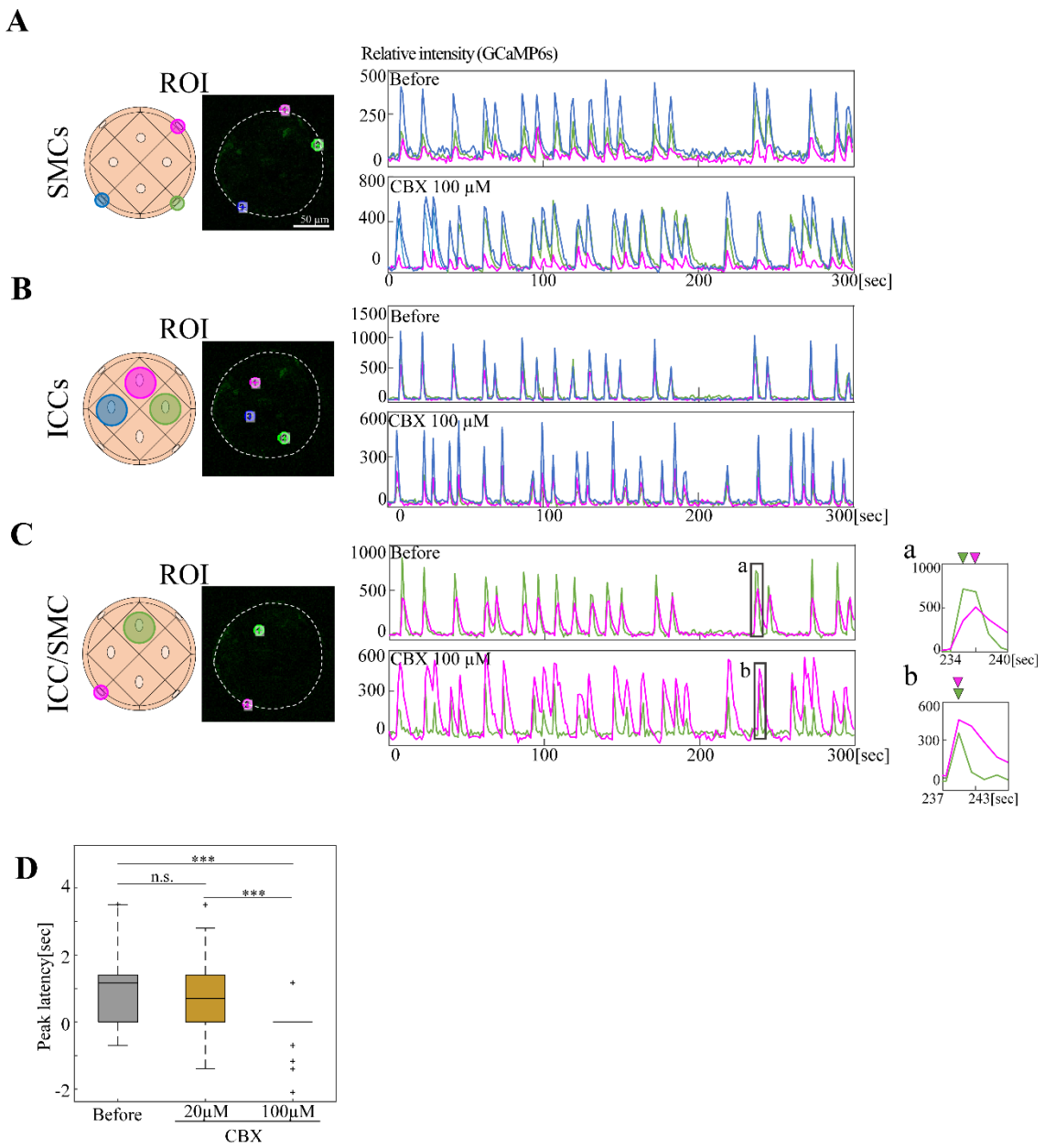

Figure 5. Gap junction inhibitor exerted limited effects on the synchronization of Ca^{2+} dynamics.

Ca^{2+} synchronization among two or three ROIs in GCaMP6s-expressing organoids was evaluated before and after treatment with 100 μM CBX. The synchronization was unaffected between **(A)** SMC-SMC and **(B)** ICC-ICC, but was partially affected between **(C)** ICC–SMC. Magnified views **(a, b)** highlight that the preceding Ca^{2+} peak in ICC (green) observed before CBX treatment (a) was abolished after treatment (b). **(D)** Peak latency between ICC and SMC. Median values: Before, 1.167; CBX 20 μM, 0.701; CBX

100 μM, 0.0. Statistical significance was assessed using Welch's t-test. ***$p < 0.001$, n.s., $p \geq 0.05$ (p = 0.27 for Before vs. CBX 20 μM). Sample sizes: Before: $n = 10$, peak count = 50; CBX 20 μM: $n = 5$, peak count = 34; 100 μM: $n = 5$, peak count = 51, Scale bar: 50 μm (A).

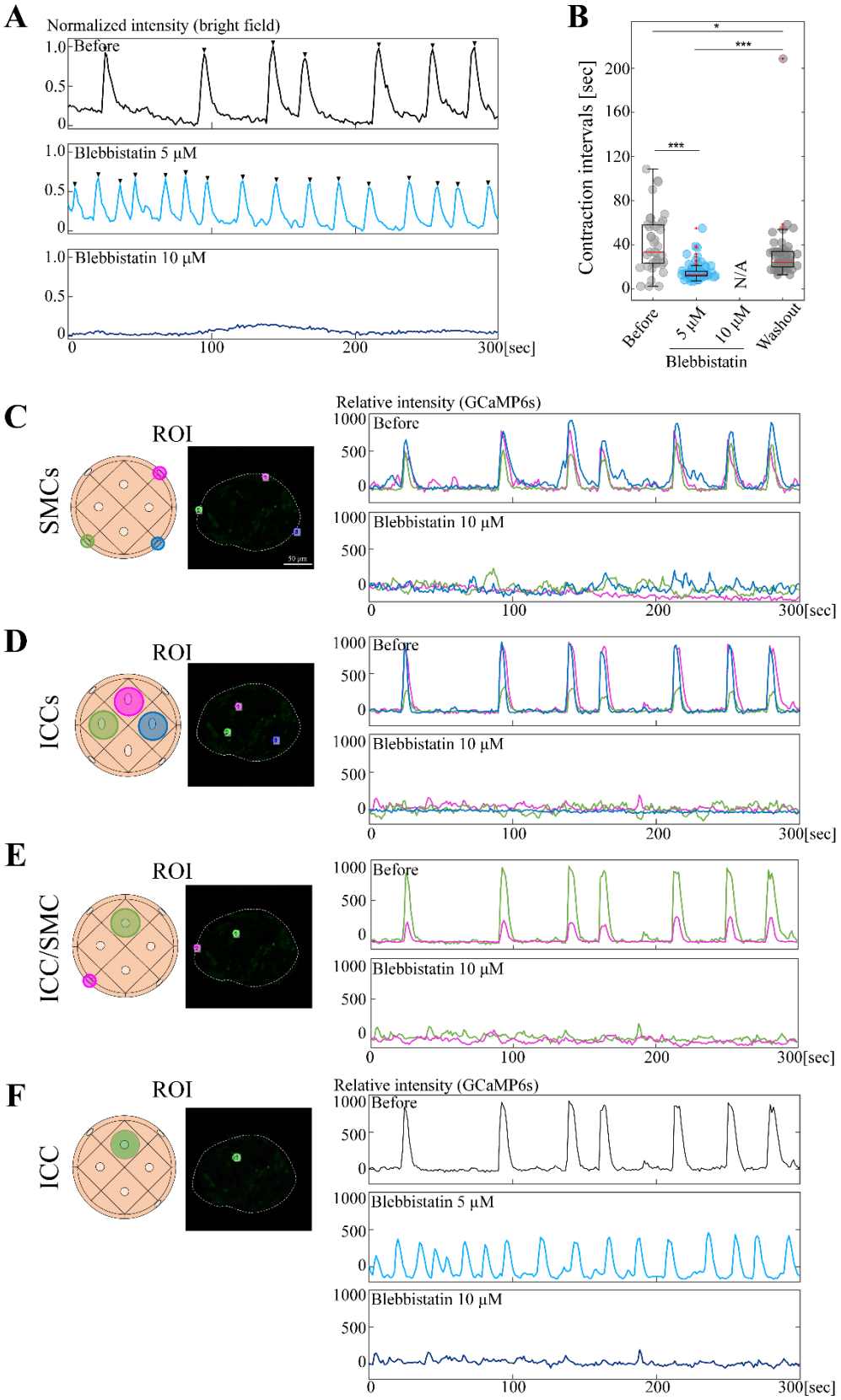
A
Normalized intensity (bright field)
Before
Blebbistatin 5 μM
Blebbistatin 10 μM
1.0
0.5
0
0
100
200
300[sec]
B
Contraction intervals [sec]
200
160
120
80
40
0
*
***
***
N/A
Before
5 μM
10 μM
Washout
Blebbistatin
C
SMCs
ROI
Relative intensity (GCaMP6s)
Before
Blebbistatin 10 μM
1000
500
0
100
200
300[sec]
D
ICCs
ROI
Before
Blebbistatin 10 μM
E
ICC/SMC
ROI
Before
Blebbistatin 10 μM
F
ICC
ROI
Relative intensity (GCaMP6s)
Before
Blebbistatin 5 μM
Blebbistatin 10 μM

798

799 **Figure 6. The organoidal contraction is important for Ca^{2+} dynamics in ICCs.**
800 GCaMP6s-expressing organoids were cultured with Blebbistatin. **(A)** Organoidal
801 contractions were extinguished at 10 μM. **(B)** Contraction intervals before and after
802 Blebbistatin, and upon washout. Median values: Before, 33.46; Blebbistatin 5 μM,
803 12.86; 10 μM, N/A; Washout, 23.95. Statistical significance was assessed using
804 Welch's t-test. ***$p < 0.001$, *$p < 0.05$. Sample size: $n = 3$. **(C-E)** Comparison of Ca^{2+}
805 dynamics in SMC-SMC, ICC-ICC, and ICC-SMC. Three or two ROIs were assessed
806 before and after administrations of 10 μM Blebbistatin. **(F)** Ca^{2+} transients in a single
807 ICC at 0 μM (before), 5 μM, and 10 μM. Scale bar: 50 μm (B).
808

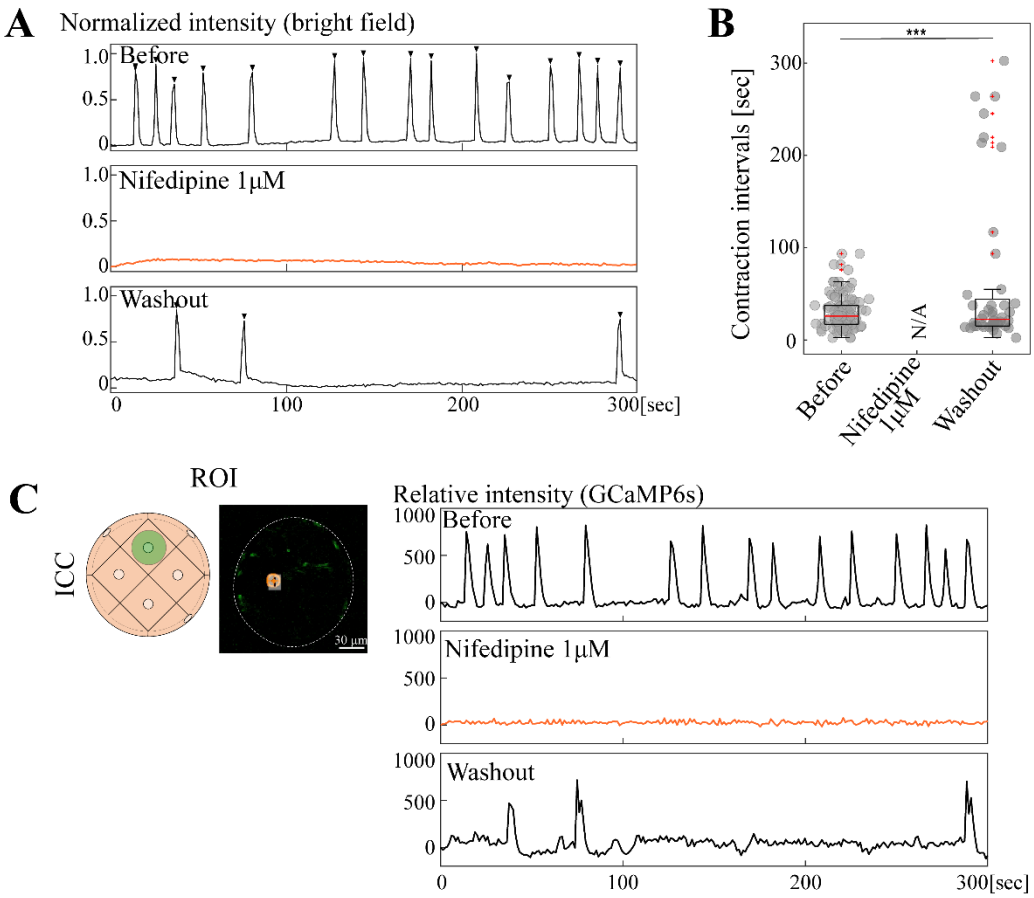

Figure 7. Nifedipine ceased organoidal contractions and Ca^{2+} activities in ICCs. Similar experiment to Fig. 6. **(A)** Organoidal contractions were extinguished at 1 μM. **(B)** Contraction intervals before and after administration, and upon washout. Median values: Before, 25.7; Nifedipine 1 μM, N/A; Washout, 22.2. Statistical significance was assessed using Welch's t-test. $^{**}p < 0.01$. Sample size: $n = 4$. Peak counts: Before, 101; Nifedipine 1 μM, N/A; Washout, 46. **(C)** Ca^{2+} transients in a single ICC before and after administration of 1 μM nifedipine, and following washout. Scale bar: 50 μm (B).

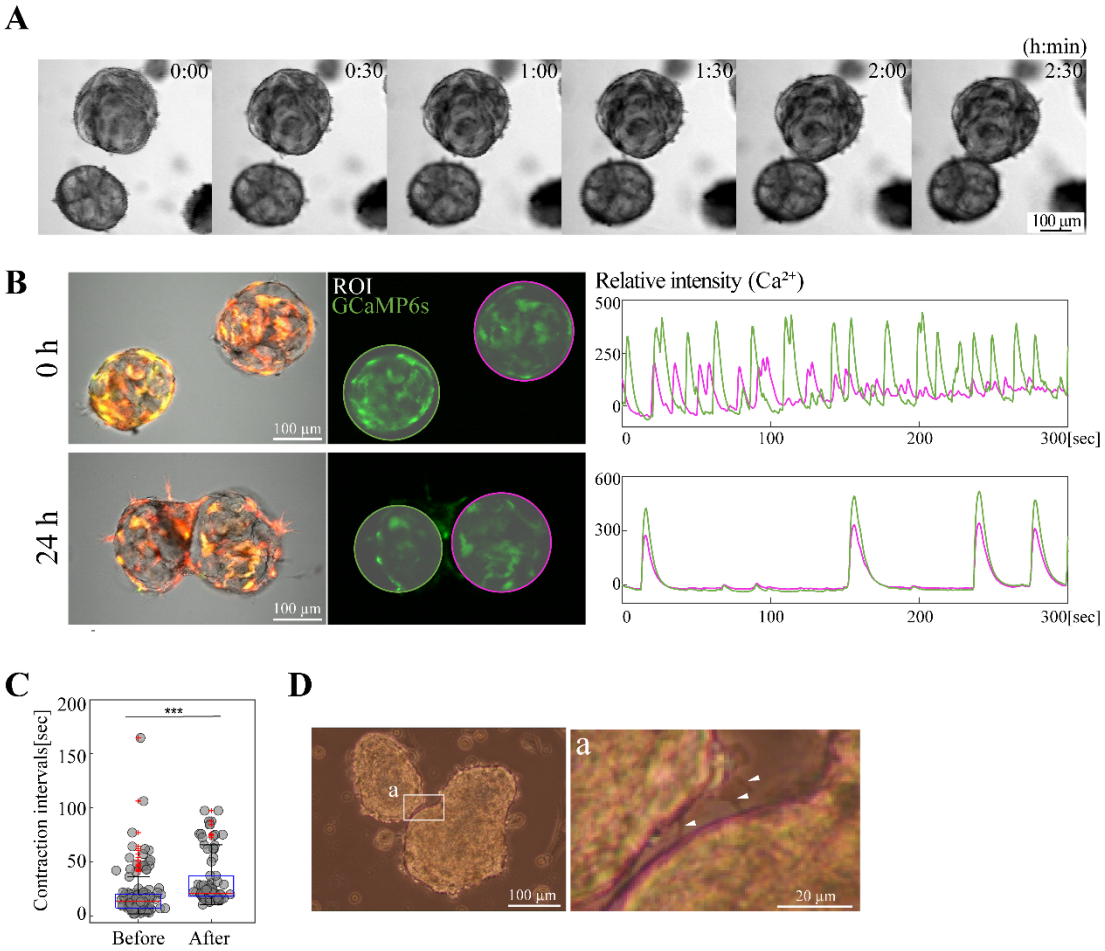

Figure 8. Ca^{2+} transients in multiple organoids undergo synchronization upon organoidal fusion.

(A) Time-lapse imaging of organoidal fusion. **(B)** When two organoids that originally displayed independent Ca^{2+} rhythm fused to each other, their rhythm became synchronized after fusion (24 h). **(C)** Contraction intervals before and after fusion. Median values: before fusion, 13.65; after fusion, 21.04. Statistical significance was assessed using Welch's t-test. ***$p < 0.001$. Sample size: $n = 3$ pairs. Peak counts: before, 138; after, 90. **(D)** Cellular protrusions between two neighboring organoids. White arrowheads show three protrusions from the left organoid. Scale bars: 100 µm (A, B, D), 20 µm (inset (a) in (D)).

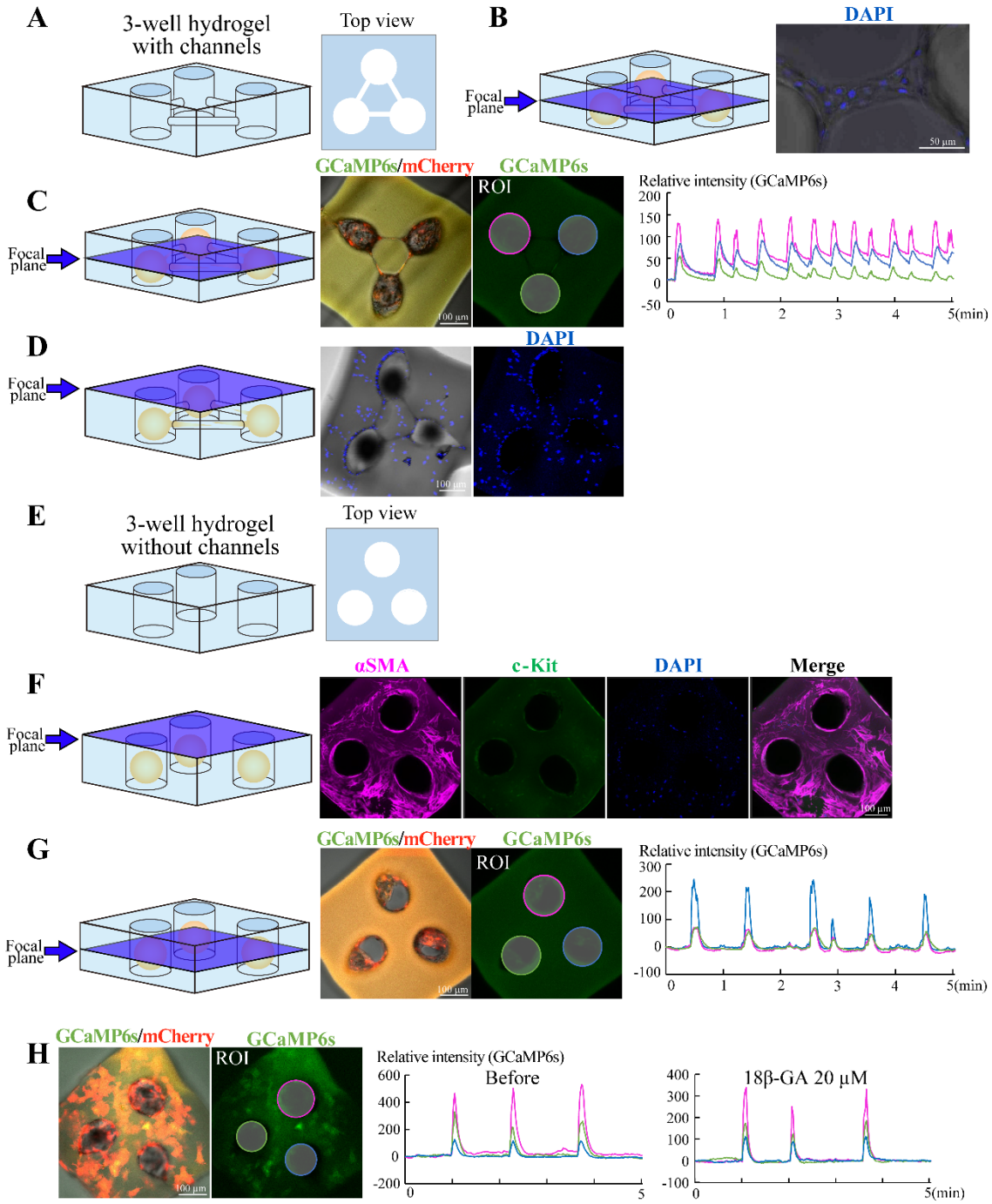

Figure 9. Smooth muscle cells mediate Ca^{2+} synchronization between organoids. **(A)** Diagram of a 3-well hydrogel in which one organoid was placed per well. The three wells were connected with narrow channels, and this gel mold does not allow organoidal bodies to fuse to each other, but allow them to extend/migrate protrusions/cells through the channel **(B)**. **(C)** After 3 days, the three organoids displayed synchronization of Ca^{2+} dynamics. **(D)** Some organoid-derived cells crawled out from the wells, and covered the top surface of the hydrogel, resulting in bridging the three unfused organoids. **(E)**

838 Diagram of a 3-well hydrogel *without* channels. **(F)** The surface-covering cells were
839 identified as SMCs (αSMA-positive, c-Kit-negative). **(G)** In the hydrogel without
840 channels but with surface-covered SMCs, Ca^{2+} dynamics in the three organoids were
841 synchronized. **(H)** The Ca^{2+} synchronization shown in (G) was not altered by treatment
842 with 18β-GA. Blue planes indicate focal planes. Scale bars: 50 μm (B); 100 μm (C, D, F,
843 G, H).
844

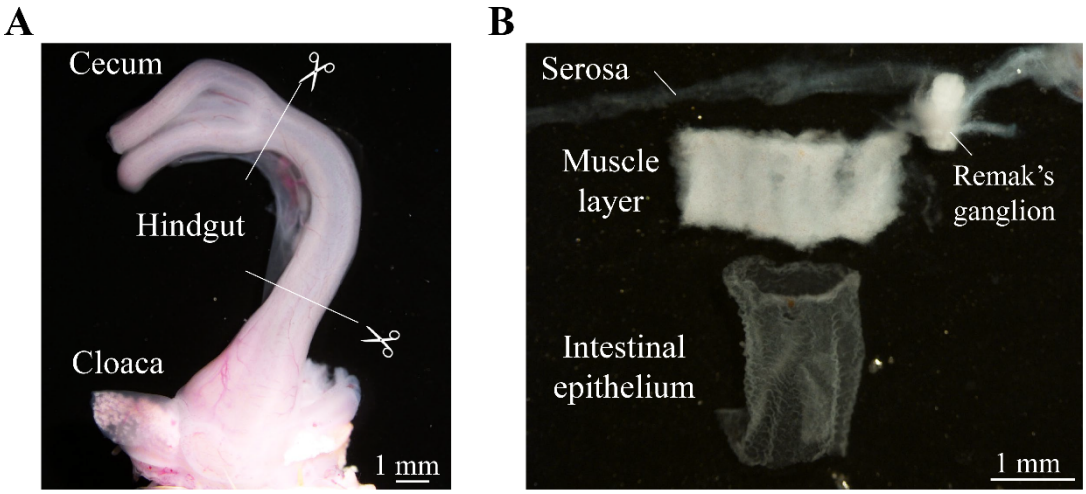

845

846 **Supplementary Figure S1**

847 (A) Chicken embryonic hindgut at E15. It was dissected from the bottom of the cecum to
848 the front of the cloaca (white lines). (B) Three layers of E15 hindgut: serosa, muscle layer,
849 intestinal epithelium. Remak's ganglion was also removed. Scale bars: 1 mm in A, B

850

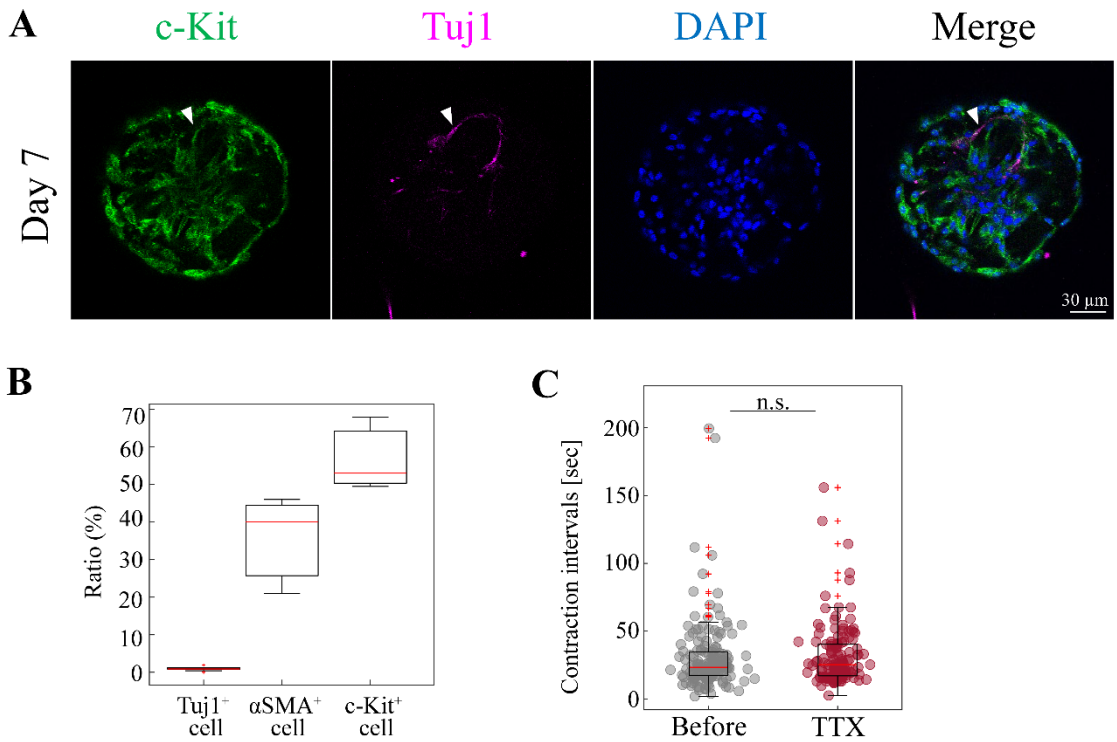

Supplementary Figure S2

(A) Co-staining of Day 7 organoids with anti-c-Kit- and Tuj1 antibodies. White arrowhead shows a Tuj1^{+} cell. **(B)** Representation of Tuj1-positive, αSMA-single positive, c-Kit-single positive cells in an organoid at day 7. Median values: Tuj1^{+}, 0.92; αSMA^{+}, 40; c-Kit^{+}, 53. Sample size: Tuj1^{+}, $n = 12$; αSMA^{+}, c-Kit^{+}, $n = 3$ **(C)** Contraction intervals before and after administration of TTX. Median values: Before, 23.4; TTX, 25.35. Sample size: $n = 9$. Peak counts: Before, 166; TTX, 148. Statistical significance was assessed using Welch's t-test. *n.s.*, $p \geq 0.05$ ($p = 0.11$). Scale bar: 30 µm (A).

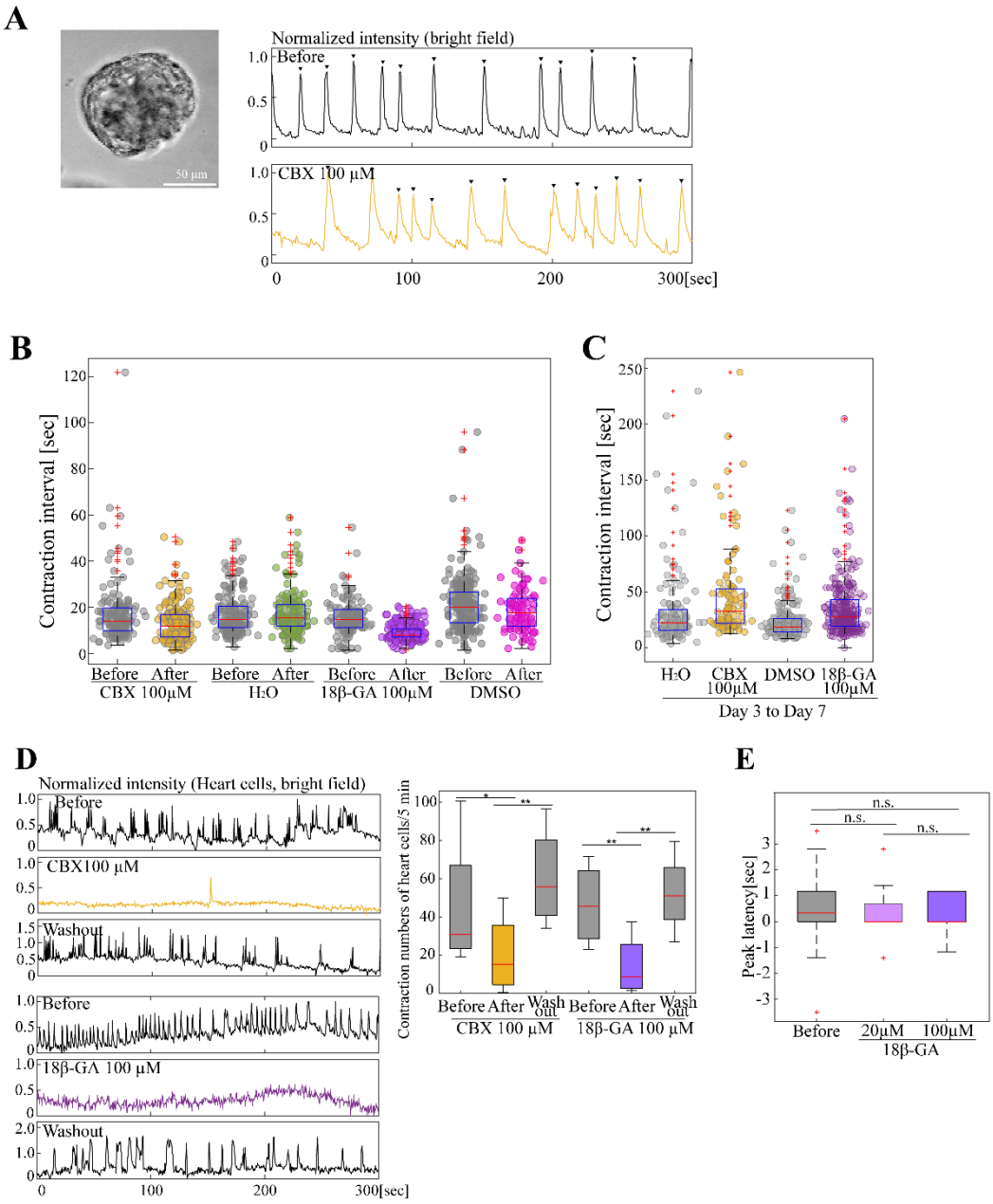

Supplementary Figure S3

Effects of gap junction inhibitors on organoidal contractions and ICC-SMC latency. **(A)** Organoids at day 7 exhibited rhythmic contractions before and after administration of 100 μM CBX. Graphs show normalized contraction intensities visualized using the Time Measurement function. Arrowheads indicate contraction peaks defined by a peak prominence > 0.25 and a peak width ≤ 10 seconds. **(B)** Contraction intervals before and after treatment with CBX (100 μM), H_2O (vehicle control for CBX), 18β-GA (100 μM), and DMSO (vehicle control for 18β-GA). Median values: CBX, 14.0 (before), 11.9

(after); H_2O, 14.7 (before), 15.4 (after); 18β-GA, 14.7 (before), 7.7 (after); DMSO, 19.95 (before), 17.5 (after). Sample sizes and peak counts: CBX, $n = 9$ (before), $n = 9$ (after), peak count = 150 (before), 196 (after); H_2O, $n = 10$ (before), $n = 10$ (after), peak count = 173 (before), 171 (after); 18β-GA, $n = 7$ (before), $n = 8$ (after), peak count = 129; DMSO, $n = 7$ (before), $n = 6$ (after), peak count = 193 (before), 92 (after). **(C)** Contraction intervals at day 7 in organoids cultured with CBX, H_2O, 18β-GA, and DMSO from day 3 to day 7. Median values: H_2O, 22.75; CBX, 32.5; DMSO, 18.85; 18β-GA, 27.95. Sample sizes and peak counts: H_2O, $n = 9$, peak count = 136; CBX, $n = 11$, peak count = 135; DMSO, $n = 9$, peak count = 209; 18β-GA, $n = 18$, peak count = 268. **(D)** Peak latency of Ca^{2+} transients between ICC and SMC before and after administration of 18β-GA (20 μM, 100 μM). Statistical significance was assessed using Welch's t-test. n.s., $p = 0.27$ for Before vs. 18β-GA 20 μM; $p = 0.25$ for Before vs. 18β-GA 100 μM; $p = 0.46$ for 18β-GA 20 μM vs. 100 μM. Sample sizes and peak counts: Before, $n = 5$, peak count = 62; 18β-GA 20 μM, $n = 3$, peak count = 52; 18β-GA 100 μM, $n = 2$, peak count = 57. **(E)** Contractions of cultured embryonic heart cells. Graphs show normalized contraction intensities using the Time Measurement function. The box plot shows the number of contractions per 5 minutes. Median values: CBX, 30.75 (before), 15(CBX 100μM), 55.75 (washout); 18β-GA: 45.5 (before), 8.5 (18β-GA 100μM), 51 (washout). Statistical significance was assessed using Welch's t-test. $^{**}p < 0.01$, $^{*}p < 0.05$; n.s., $p \geq 0.05$ ($p = 0.13$ for Before vs. washout of CBX; $p = 0.26$ for Before vs. washout of 18β-GA). Sample sizes: CBX, $n = 4$; 18β-GA, $n = 4$. Scale bar: 50 μm (A).

892
893 **Movie 1**
894 Long-term time-lapse imaging after seeding. Time lapse was taken every 2 hours
895 for a total of 100 hours. This video corresponds to Fig. 1B.
896
897 **Movie 2**
898 Periodic contractions of the cluster/spheroid on day 3, 5 and 7. Time-lapse images
899 were taken with 700 msec intervals for 5 min. This video corresponds to Fig. 2A.
900
901 **Movie 3**
902 Periodic contractions of a day 7 organoid with CBX. Time-lapse images were
903 obtained with 700 msec intervals for 5 min. This video corresponds to Fig. S3.
904
905 **Movie 4**
906 Ca^{2+} dynamics in day 7 gut contractile organoid are concomitant with its
907 contractions. Time-lapse images were obtained with 700 msec intervals for 5 min. This
908 video corresponds to Fig. 4.
909
910 **Movie 5**
911 Ca^{2+} dynamics in a gut contractile organoid with CBX. Time-lapse images were
912 obtained with 700 msec intervals for 5 min. This video corresponds to Fig. 5.
913
914 **Movie 6**
915 Ca^{2+} dynamics in day 7 gut contractile organoid with Blebbistatin. Time-lapse
916 images were obtained with 700 msec intervals for 5 min. This video corresponds to Fig.
917 6.
918
919 **Movie 7**
920 Live imaging during fusion of multiple organoids. Time-lapse images were
921 obtained every 10 minutes for 4 hours. This video corresponds to Fig. 8A.
922
923 **Movie 8**
924 Ca^{2+} transients in two gut contractile organoids before and after fusion. Time-
925 lapse images were obtained with 450 msec intervals for 5 min. This video corresponds to
926 Fig. 8B.
927

928 **Movie 9**

929 Ca^{2+} transients in three gut contractile organoids in 3-well hydrogel with channels.
930 Time-lapse images were obtained with 700 msec intervals for 5 min. This video
931 corresponds to Fig. 9C.

932

933 **Movie 10**

934 Ca^{2+} transients in three gut contractile organoids in 3-well hydrogel *without*
935 channels. Time-lapse images were obtained with 450 msec intervals for 5 min. This
936 video corresponds to Fig. 9G.

937

938 **Movie 11**

939 Similar assay to movie 10 with 18β-GA administration. Time-lapse images were
940 obtained with 700 msec intervals for 5 min. This video corresponds to Fig. 9H.